Metallaaromatic complexes as candidates for future molecular materials and electronic devices: recent advancements

Article

Accepted Version

Metallaaromatic complexes as candidates for future molecular materials and electronic devices: recent advancements

Xiao Fei Yang,[a,†] Ming-Xing Zhang,[a,b,†] Sheng Hua Liu*[,a] and František Hartl*[,c]

[a]*National Key Laboratory of Green Pesticide, College of Chemistry, Central China Normal University, Wuhan 430079, PR China.*

[b]*Hubei Key Laboratory of Purification and Application of Plant Anti-cancer Active Ingredients, College of Chemistry and Life Science, Hubei University of Education, Wuhan, 430205, China*

[c]*Department of Chemistry, University of Reading, Whiteknights, Reading RG6 6DX, United Kingdom*

† These authors contributed equally to this work.

ABSTRACT

In recent years, the field of organometallic chemistry has made a great progress and diverse types of metallaaromatics have successively been reported. In those studies, incorporation of ligated osmium(II) centers into metallaaromatic systems played a prominent role. The reviewed literature documents that certain metallaaromatics with unconventional photophysical properties, redox and electronic transport properties and magnetism, have potential to be widely used in diverse practical applications, with selected examples of amino acid identification, photothermal effects, functional materials, photodynamic therapy (PDT) in biomedicine, single-molecule junction conductors, and electron-transport layer materials (ETLs) in solar cells.

1. INTRODUCTION

Since Kekulé first proposed the concept of "aromaticity" in 1865,[1,2] the field of organic aromatic compounds has been growing rapidly. Polycyclic aromatic hydrocarbons (PAHs) have widely been implemented in organic field-effect transistors, organic

semiconducting materials, organic light-emitting diodes, etc., due to their highly delocalized, π-conjugated planar structure, high stability and suitable optoelectronic properties.[3-12] However, their exploration often brings about also shortcomings, such as tedious synthetic procedures, low reaction yields, and poor solubility, thereby limiting the applicability. Introduction of some main-group elements may affect energies of the frontier orbitals of the heteroaromatic molecules and increase their stability and solubility to some extent, realizing high performance p-channel field effect transistors.[13-21] Metallaaromatics[22] can be broadly defined as aromatic complexes containing metal atom(s) in an aromatic ring, and considered as combinations of organometallics and conventional organic aromatics. They have attracted widespread attention for their structural diversity, novelty, and transient properties of metal complexes and organic aromatic compounds.

The advantages of metallaaromatics over PAHs are mainly manifested in the following behavior. i) The involvement of metal valence *d*-orbitals and diverse types of auxiliary ligands on the metal center will not only stabilizes organic anti-aromatic compounds as well as small cyclic alkynes or carbenes,[23] but also lay the foundation for the realization of functional materials.[24,25] ii) As a special class of aromatic compounds, steric hindrance of metal centers and their auxiliary ligands affects the molecular packing mode,[23] thereby improving photophysical properties[26] and regulating optical properties, which are widely used in photothermal effects,[27] biomedicine[28] and other fields. iii) The d_{π}-p_{π} conjugation or hyperconjugation reached via an efficient orbital overlap between Os−d_{xy} [29] and p_{π} orbitals and the strong π-π interactions between molecules of the PPh_3 ligand itself, [30] giving it stronger electronic transport properties. The excellent electronic transport properties enable metallaaromatics to be used as candidates for electron-transport layer materials (ETLs) in single-molecule conductors [29] and solar cells.[30] iv) The importance of metallapyridines, metallapyridiniums and metallapentalenes with a transition metal and phosphonium substituents in achieving adaptive aromaticity (species with aromaticity in both the ground state and the excited state).[31-33] The triplet ground state was found through calculations[31] and may preserve the possibility for the discovery of more

organometallics towards photochemical and molecular magnetic applications. Therefore, metallaaromatics offer a considerable development space and application prospects.

Thorn and Hoffman first predicted the existence of three types of metallabenzenes in 1979 and explained their aromaticity with π electron delocalization rules.[34] Three years later, Roper and colleagues reported the first transition metallaaromatic complex, osmabenzene,[35] which became a milestone for metallaaromatics, laying the foundation for subsequent expansion of the metallaaromatics family. In the past few decades, metallaaromatics made a major breakthrough in their development and a variety of metallaaromatics (Ni, Ru, Ta, W, Os, Ir, Pt, Re, etc.) have been reported. In addition to metallacyclobutadienes,[36-41] dimetallaaromatics,[42-44] metallacyclopropenes[45-46] and dicupra[10]annulenes,[47-49] six major types of metallaromatics, viz. metallabenzenes,[50] metallabenzynes,[50-53] heterometallaaromatics,[54-57] dianion metalloles,[58-61] metallapentalenes and metallapentalynes (also termed carbolongs),[62] and spiro metalloles,[60] have been reported and extensively studied. Heterometallaaromatics include metallafurans,[61-70] metallapyrroles,[71-72] metallathiophenes,[72-75] metallapyryliums,[76-78] metallapyridines and metallapyridiniums,[79] metallathiabenzenes[80-82] and other heterometallaaromatics.[83-88]

In recent years, most of the comprehensive publications have commented on the structure, synthesis methods, aromaticity, reactivity of metallaaromatics and the importance of density functional theory calculations for the development of metallaaromatics.[50, 55, 60-62, 89-91] The physico-chemical properties and potential applications of metallaaromatics are almost not covered. Until 2020, Xia's group briefly mentioned the application of metallaaromatics in catalysis, materials, medicine and other aspects.[22] In 2023, Xia's group showcased in detail the recent advances in applications of carbolong complexes based on their different properties.[92] However, the physico-chemical properties and the potential applications of other types of metallaaromatics need to be supplemented, especially the aspect of combining calculations to rationalize the physico-chemical properties of metallaaromatics.

Based on this information, in the following text, we focus more on the state-of-

the-art in the realm of physico-chemical properties of metallararomatics in selected examples of metallofurans, metallapyrroles, metallabenzenes, metallanaphthalenes, metallapentalenes, and metallapentalynes and their derivatives (Figure 1). The catalytic properties of metallaaromatics are not discussed here. The discussed applications regard pioneering reports on amino acid identification, optoelectronic devices, functional materials, agents in biomedicine, single-molecule conductors, solar cells, etc.

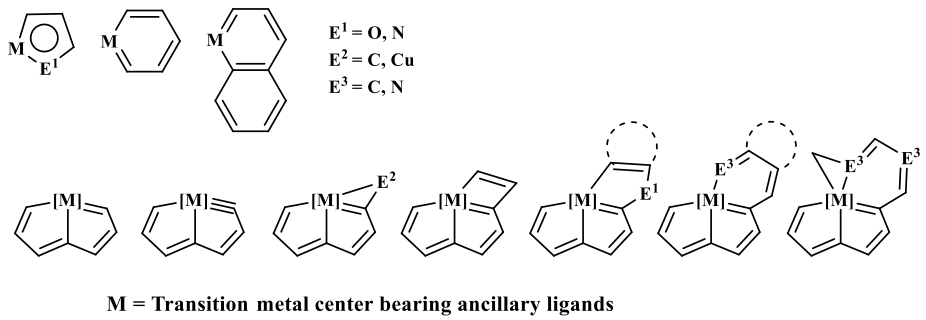

Figure 1. Structural types of metallaaromatics discussed in this review.

2. PHOTOPHYSICAL PROPERTIES OF METALLAAROMATICS: EXAMPLES AND APPLICATION

2.1 Photophysical properties

In 2011, the Xia's group studied nucleophilic aromatic substitution of ruthenabenzenes and synthesized their isomeric derivatives **1** (greenish-yellow) and **2** (green) in a single-step reaction with 8-hydroxyquinoline (Figure 2A).[93] Crystallographic data of **1** and **2** have revealed the six-membered ruthenabenzene ring and two 8-hydroxyquinolines, one chelating at the Ru center and the other one tethered to the ruthenacyclic system in a co-planar fashion, resulting in strongly delocalized π-bonding. These isomer complexes emit light in common organic solvents, with photoluminescence quantum yields reaching 0.01 and 0.04 for **1** and **2** in methanol/water 1:1 (v/v), respectively. Interestingly, similar to conjugated organic fluorophores such as fluorescein and rhodamine green dyes, the Stokes shifts for complexes **1** and **2** are relatively small (about 700 cm^{-1}), as shown in Figure 2B. The photoluminescence lifetimes have not been determined and the exact nature of the emitting excited states remains to be

highlighted.

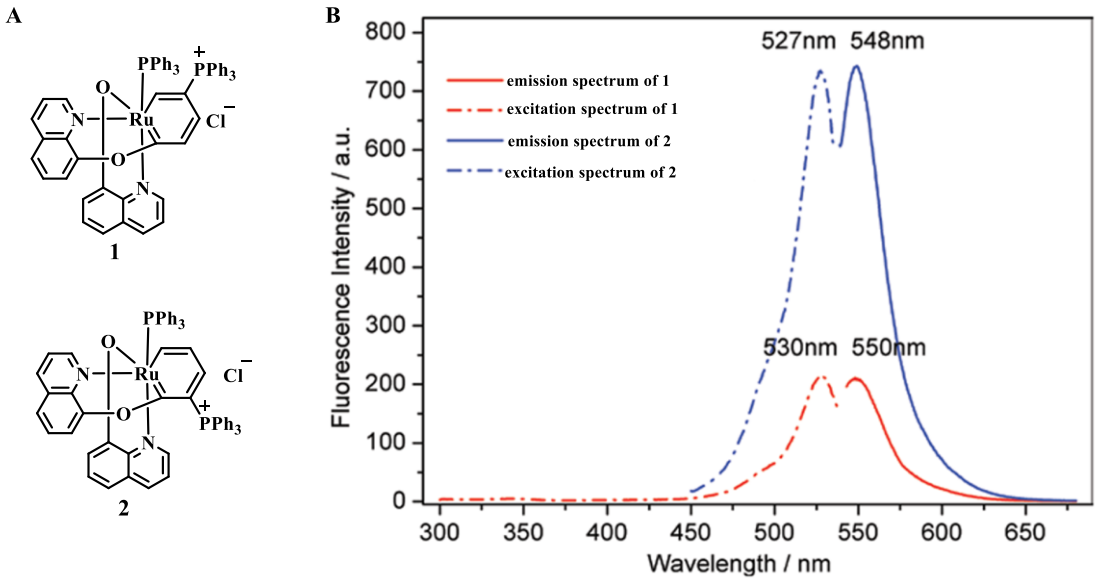

Figure 2. A) Schematic molecular structures of ruthenabenzenes **1** and **2**. B) Excitation (dashed line) and emission (solid line) spectra of **1** and **2** (10^{-4} mol mol^{-3}) in methanol/water 1:1 (v/v).

In 2013, Xia and co-workers synthesized the first five-membered cyclic metal carbyne complex, viz. osmapentalyne **3** (Figure 3A).[23] Both experimental and theoretical data have confirmed its aromaticity. This pioneering work has thus extended the aromaticity concept to five-membered rings featuring an M≡C bond and 4 delocalized π-electrons (Craig/Möbius type). Complex **3** shows a band at 440 nm in the excitation spectrum at room temperature (Figure 3B) and displays unusual aggregation-enhanced near-infrared photoluminescence with a remarkably large Stokes shift and long lifetime. Since the bulky PPh_3 ligands on Os(II) suppress π-π stacking, the photoluminescence intensity of **3** was gradually enhanced upon the addition of water to the ethanol solution, overcoming the shortcomings of aggregation quenching[94] in traditional conjugated polycyclic aromatic systems. Therefore, osmapentalyne **3** is a promising near-infrared dye.

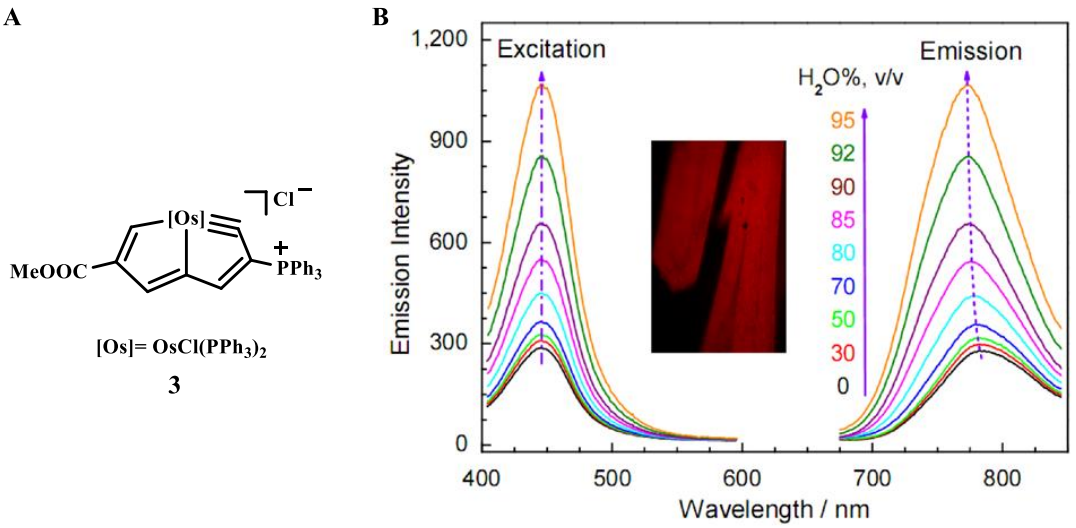

Figure 3. A) Schematic molecular structure of osmapentalyne **3**. B) The aggregation-induced enhancement of long-lived luminescence of 10^{-4} M **3** in ethanol/water. The excitation wavelength was 440 nm.

A remarkable series of luminescent heterocyclic iridium(III) complexes **7**–**16** was prepared from hydridovinyliridium precursors **4**–**6** (Figures 4A, 4B).[95] Tuning the energy of the LUMOs and HOMOs of these complexes was successfully achieved by a synergetic modification of substituents on the 2,2'-bipyridine ligand and the benzene ring of the iridabenzocyclopentadiene system. Theoretical calculations have shown that the chelating α-diimine ligand mainly affects the LUMO energy that is rising with electron-donating groups. On the contrary, the substituents on the benzene ring mainly affect the energy of the HOMO. Electron-withdrawing bromo and fluoro substituents reduce the electron density at the iridacycle, thereby stabilizing the HOMO. Controlling the energy of the frontier orbitals in the series has a strong impact on the phosphorescence seen after the MLCT/LLCT excitation in the visible region (400–500 nm), as confirmed experimentally (Figure 4C). Complex **8** contains a more rigid 1,10-phenanthroline ligand instead of 2,2'-bipyridine in **7** and its phosphorescence becomes blue-shifted compared to the latter complex. The emission maximum of **9** bearing the donor *t*-butyl groups in the 4,4'-positions at the 2,2'-bipyridine ligand is markedly blue-shifted compared to that of **7**, whilst red-shifted for **10** bearing the electron-withdrawing bromo substituents. Notably, strongly red-shifted visible absorption and phosphorescence are achieved by the replacement of the benzene ring in the

iridapolycyclic system of **7** with the thiophene ring in **16** (Figure 4C). In line with the energy gap law, the phospohorescence quantum yields of **10** (0.096) and **16** (< 0.01) are strongly reduced compared to **9** (0.48) and **12** (0.64). Apparently, this class of complexes with a flexible iridapolycyclic architecture bearing the triphenylphosphonium group have a potential to serve as phosphorescent materials, with an accent on biosensing probes.

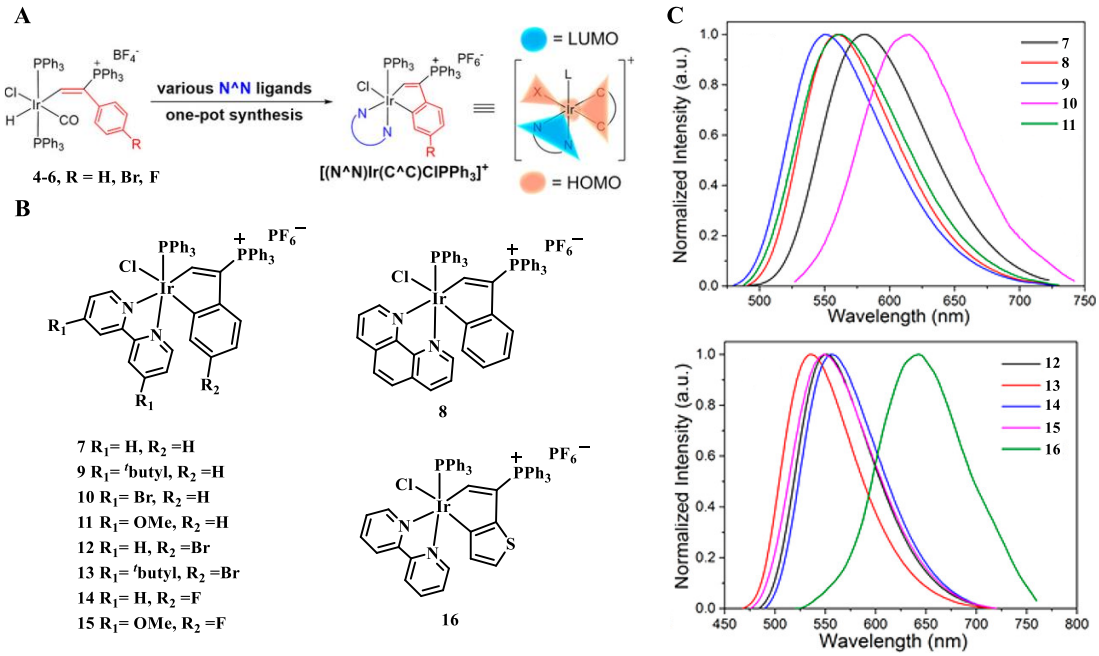

Figure 4. A) The synthetic route to iridapolycyclic complexes. B) Schematic molecular structures of iridapolycyclic complexes **7**–**16**. C) Tunable phosphorescence of **7**–**16** in dichloromethane at room temperature.

Carbolong complexes represent a new field of organometallic chemistry of coplanar polycyclic (pincer-type) frameworks formed by 7C (for metallapentalyne) to 12C chains coordinated to the central metal by at least three carbon atoms.[62] Carbolong complexes are generally highly reactive in solution but stable in the solid state. Their potential applications in materials research and biomedicine have been investigated.[24,28] In 2018, aromatic ruthenapentalyne **17** (Figure 5A) was synthesized by a single-pot reaction as the first representative of a 4*d* transition metal cyclic carbyne complex. It also served as a precursor in the successful syntheses of ruthenapentalene complexes **18**–**22** (Figure 5A).[96] Their electronic absorption spectra show rich and fairly intense

absorption features covering the whole visible region, i.e., 400–700 nm (Figure 5B). They deserve to be analyzed in a greater detail by time resolved spectroscopic and theoretical methods to obtain a clearer picture of the electronic structure and the nature of the optically populated excited states. In general, the electronic absorption properties of the novel ruthenapentalyne and its derivatives can be controlled effectively by structural modifications. This work may serve as a valuable reference for better understanding of the relationship between the optical properties and molecular structure of cyclic metal-carbyne and -carbene complexes.

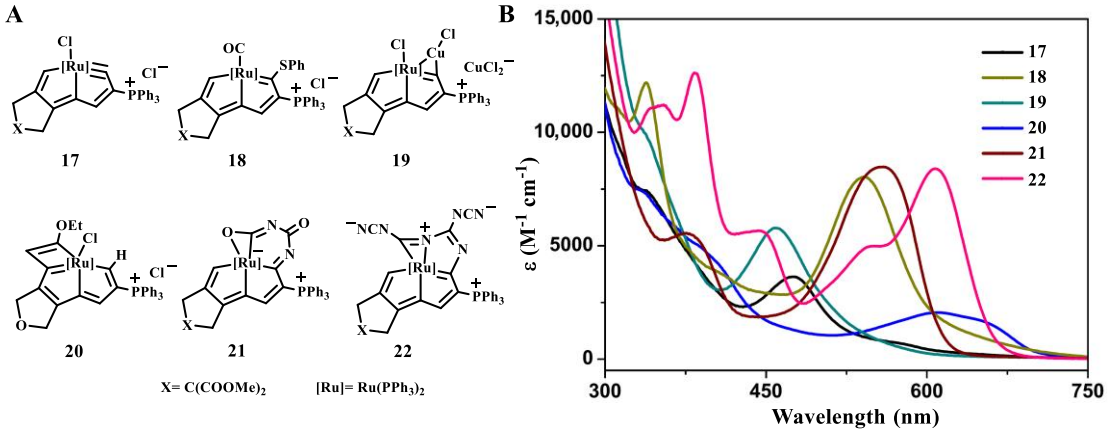

Figure 5. A) Schematic molecular structures of ruthenapolycycles **17**–**22**. B) UV-Vis absorption spectra of **17**–**22** in dichloromethane.

Conjugated polymers usually require strategies to expand the range of wavelengths absorbed and increase their solubility. Developing effective strategies to enhance both properties remains challenging. Aromatic and heteroaromatic compounds can be useful components of conjugated polymers. Metalaaromatics may also be interesting in this regard. The Xia's group prepared metalaaromatic conjugated polymers from a series of monomers **23**–**27** featuring a metallabicycle and a terminal alkyne with diverse spacer groups serving as the building blocks for conjugated polymers.[26] As shown in Figure 6A, treatment of monomers **23**–**27** with $HCl{\cdot}Et_2O$ afforded polycarbolongs **28**–**32** (Figure 6B). These polymers offer a good solubility and limited π-π stacking due to the bulky ligands on the metal (PPh_3), and display wide and strong UV-visible absorption between 500–800 nm (Figure 6C) reflecting a high degree

of electron delocalization. This work not only solves the problem of poor solubility of conjugated polymers, but also presents excellent electronic properties envisaged to offer potential applications in catalysis, optoelectronics, and biotherapeutics.

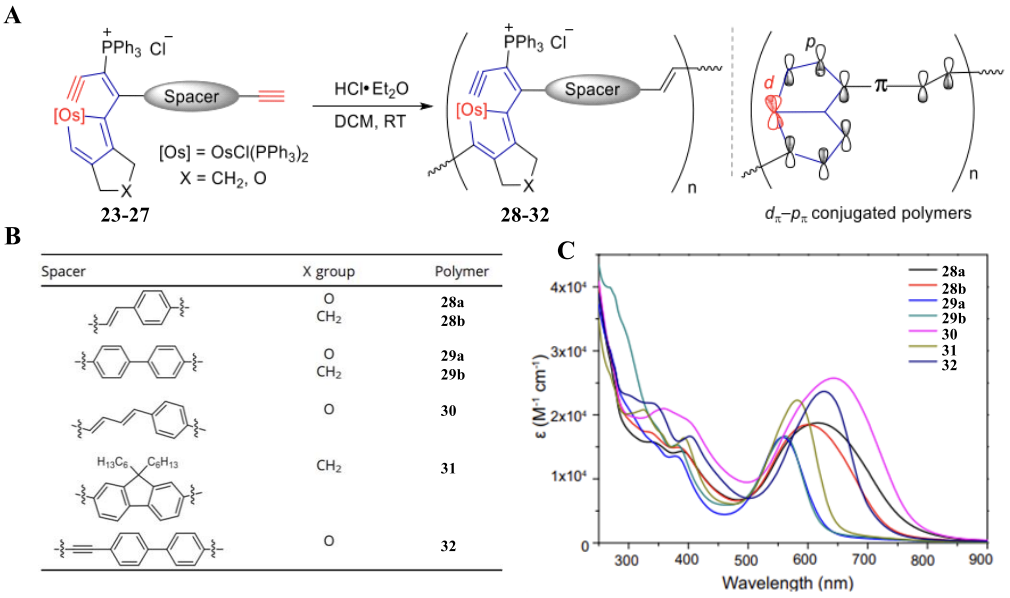

Figure 6. A) General representation of the polymerization process. B) Schematic molecular structures of polycarbolongs **28**–**32**. C) UV-Vis absorption spectra of 10^{-5} M polycarbolongs measured in DCM at RT. Molar absorption coefficients were calculated based on repeat units.

2.2 Applications

2.2.1 Amino acid identification

In 2011, a pioneering study was reported by Xia and co-workers on the application of a metallabenzene as a sensor (metallareceptor) for the detection of bioactive molecules.[24] Ruthenabenzene **33** shows a high selectivity for binding L-cysteine. Both UV-Vis absorption and photoluminescence spectra of **33** exhibit significant responsive characteristics (Figures 7B and 7C). Due to the high optical sensitivity of **33** acquired by the chelating 1,10-phenanthroline ligand, the detection limit of L-cysteine has reached the remarkable level of 10^{-5} mol dm^{-3}. The olive color of **33** turned yellow-brown on addition of L-cysteine and enhanced luminescence was observed. Other aminoacids, such as L-alanine, L-cystine or L-homocysteine, are much less responsive. This outstanding response to L-cysteine has been ascribed to the formation of the thermodynamically favored five-membered chelate ring in **33** created by the chelating

N,*S*-coordination of L-cysteine to the ruthenium center (Figure 7A). The study has laid the foundation for application of metallaaromatics in the field of (optically active) biopharmaceuticals.

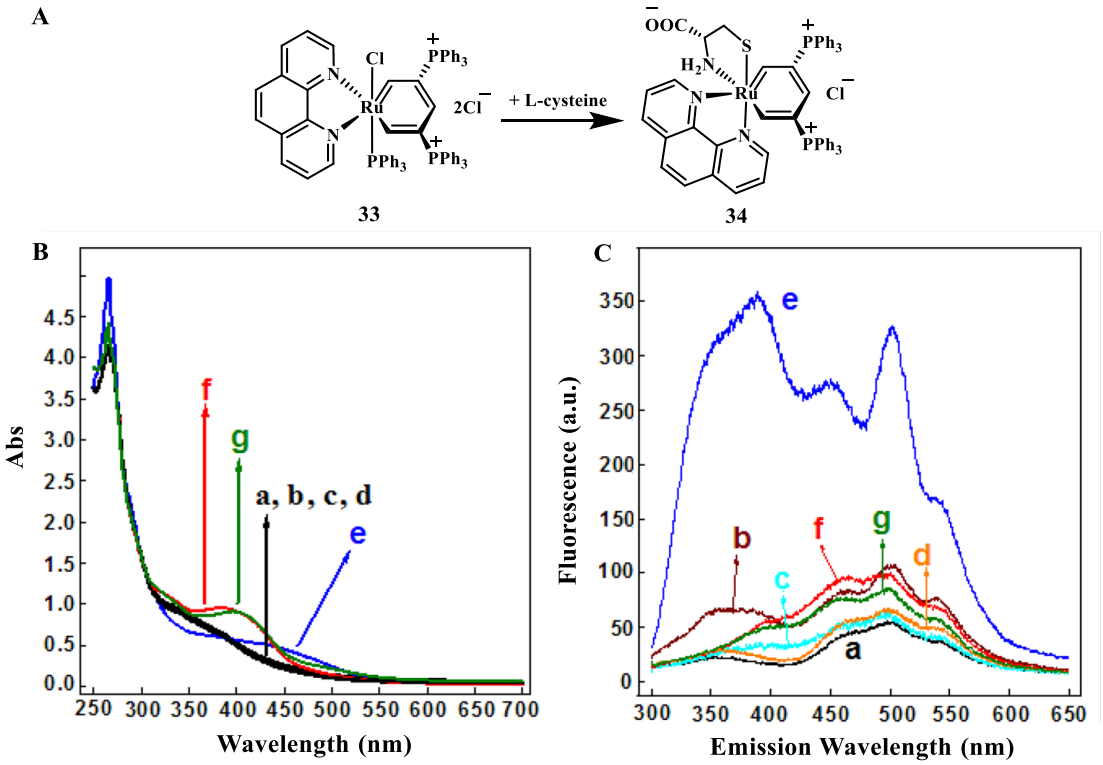

Figure 7. A) Ruthenabenzene **33** as a selective receptor of L-cysteine. Spectral responses of **33** to different amino acids at room temperature and pH 7.4 after 30 min incubation. Concentration: 8×10^{-4} mol dm^{-3}. B) UV-Vis absorption spectra: a) blank reference **33**; b) L-alanine; c) L-methionine; d) L-cystine; e) L-cysteine; f) glutathione; g) L-homocysteine. C) Photoluminescence measured upon 250-nm excitation: a) and c)–g) as given in A; b) mercaptoacetic acid.

2.2.2 Photothermal response

One of the important strategies to promote the development of materials and energy science is the structural design and performance adjustment of metallaaromatics. In 2022, Xia's group reported for the first time that $AgBF_4$ activated the C3−H site of anthranil, which in turn undergoes unconventional [3+3] cycloaddition with **35** by $C(sp^2)$−$C(sp^3)$ coupling, leading to the formation of **36**.[27] The product is not only an unusual tetracyclic metallaaromatic compound containing quinoline and pentalene motifs fused by a metal-bridged fragment, but also represents the first reported osmaquinoline (Figure 8A). The UV-Vis-NIR absorption spectrum of **36** showed an

absorption band extending to the near-infrared region (NIR-I and NIR-II) compared to the maximum absorption of **35** at 437 nm; metallaaromatics absorbing in NIR-II (important for photothermal applications) were realized for the first time in this work (Figure 8C). Theoretical calculations show that the red shift of the absorption band of **36** is caused by the cyclic d_{π}–p_{π} conjugation that can effectively reduce the HOMO–LUMO gap (Figure 8B). Not surprisingly, the photothermal conversion efficiency (PCE) value for **36** was calculated according to the change in the temperature and photothermal stability in the NIR-II region was verified by repeatedly performing six heating and cooling cycles under 1060-nm laser irradiation (Figures 8D and 8E). It is worth noting that the NIR absorption intensity as well as the photothermal properties can be adjusted by changing substituents on the conjugated aromatic rings. The stronger absorption intensity of **37** at 925 nm relative to **36** is due to introduction of a methoxy group to the tetracyclic aromatic framework, consistent with the optical excitation wavelength (λ = 895 nm) and the corresponding oscillator intensity (f = 0.0590) calculated by time-dependent density functional theory (TDDFT). Compared to the PCE value of **36**, MeO-substituted **37** can even reach 39% (Figure 5C). Thus, a cyclic d_{π}–p_{π} conjugation strategy involving the overlap of the transition metal *d*-orbitals has been demonstrated for extending the absorption, providing a new perspective for the design of NIR-II absorption molecules. At the same time, the modified skeleton provides ideas for improving its photoelectric properties.

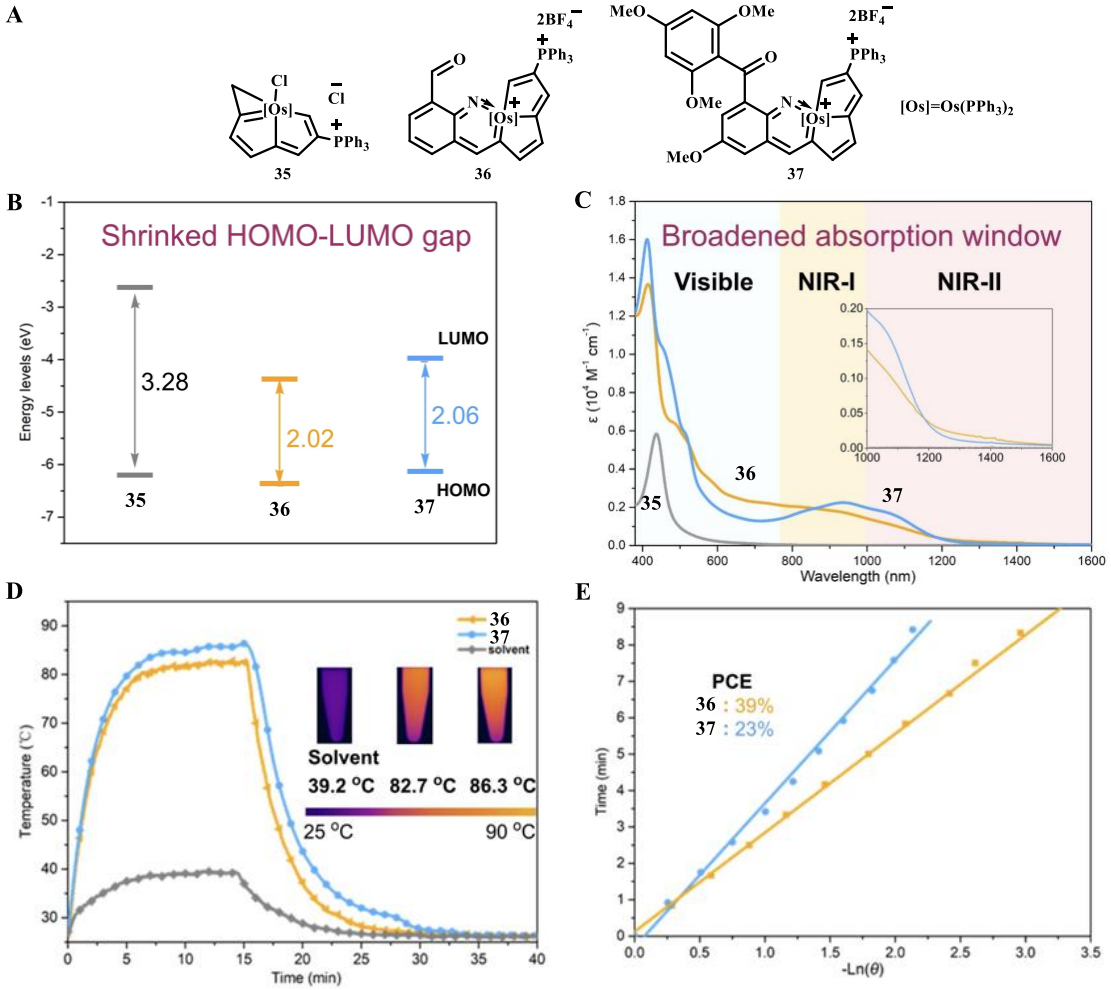

Figure 8. A) Schematic molecular structures of cyclopropa-osmapentalene **35** and condensed osmaquinolines **36** and **37**. B) The HOMO–LUMO gaps. C) Electronic absorption spectra of **35**–**37**. D) Photothermic heating curves of **36** and **37** (1.0 mg mL^{-1}) under 1060-nm (1.0 W cm^{-2}) laser irradiation for 15 min, followed by cooling to room temperature and infrared imaging of **36** and **37**. E) Linear correlation of the cooling times versus negative natural logarithm of driving force temperatures and PCEs.

2.2.3 Functional materials

In 2022, the Xia's group exploited the photothermal effect of carbolong complex **38** to combine with the thermal responsiveness of the semi-crystalline polymer chain, a polyurethane-based shape-memory polymer (SMP), and the covalent bonding of free radical exchangeability (based on the alkoxyamine fraction of TEMPO) to construct a novel SMP with a reconfigurable network.[25] It breaks the limitation that SMPs cannot be reconfigured arbitrarily to adapt to variant application scenarios. The specific implementation mechanism involves the reconfigurable shape-memory behavior of

remote control by 808-nm NIR irradiation (Figure 9).

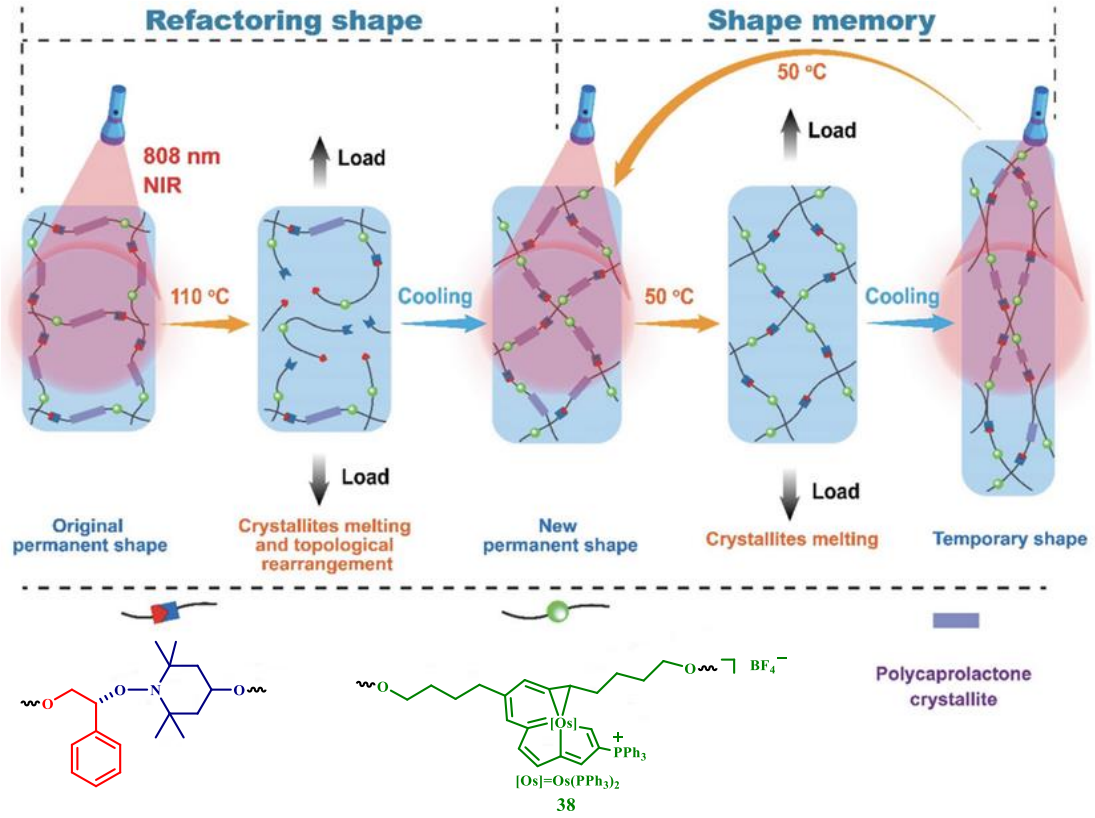

Figure 9. Schematic illustration of the optically reconfigurable shape-memory of the polymer network implementing carbolong complex **38.**

2.2.4 Biomedicine

The practical application of photodynamic therapy (PDT) is hampered by poor efficacy in hypoxia and refractory solid tumors. Of course, some metal complexes that exhibit excellent PDT effect on hypoxic tumors have also been reported.[97–103] In 2022, the Xia's group proposed a promising strategy for treating hypoxic tumors with metal-based drugs, and found that osmium–peroxide complex **40**, which remains structurally stable in the dark, can inhibit the growth of hypoxic tumors. Upon photoactivation with 465-nm light, **40** releases $O_2^{\bullet-}$ even under severely hypoxic conditions (1% O_2), and becomes transformed into cytotoxic **39** in a Cl^- containing phosphate-buffered saline (PBS) solvent (Figure 10A), thus maintaining useful photoactivation efficacy in hypoxia. Under light irradiation, **40** significantly reduces the expression of GPX4 and the enzymatic activity of NADH, leading to the accumulation of lipid peroxides, which

could effectively be inhibited by Ferrostatin-1 (Fer-1, an inhibitor of iron death) (Figures 10B–E). All of the above results confirm that **40** induces ferroptosis. Furthermore, **40** can photocatalytically oxidize endogenous NADH in living cancer cells, triggering ferroptosis (Figure 10E). In vivo studies confirm that **40** effectively inhibits the growth of solid hypoxic tumors in mice (Figure 10F).[28]

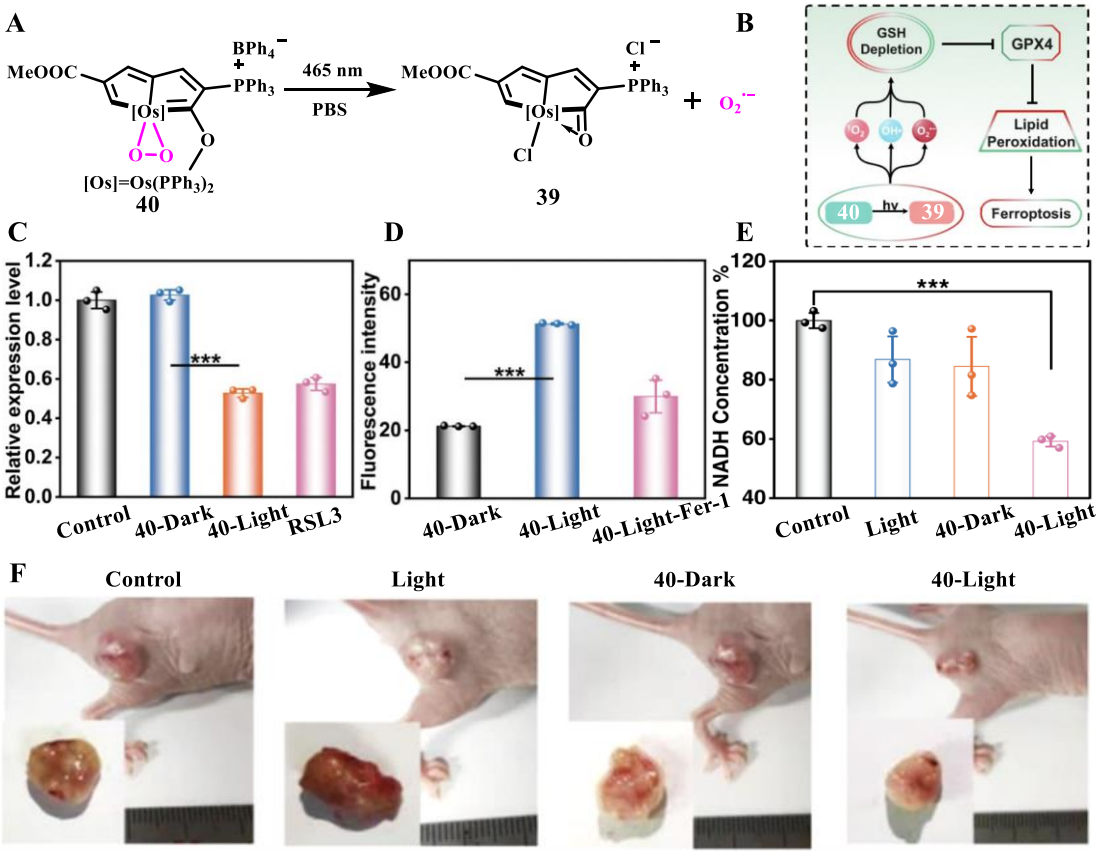

Figure 10. A) The emission spectra for monitoring $O_2^{\bullet-}$ generation by 10 μM **40** using a DHR123 probe (10 μM, λ_{exc} = 488 nm) in normoxia. B) The process of ferroptosis in this photoactive antitumor therapy. Light irradiation: 465 nm, 13 mW cm^{-2}. GSH glutathione, Fer-1 ferrostatin-1, GPX4 glutathione peroxidase 4. C) The relative expression levels of GPX4 calculated. D) The average fluorescence intensities. The experiment was repeated three times independently with similar results, p = 0.000024. E) NADH concentrations in the treated HeLa cells. **40**: 20 μM, 310 K, 8 h. All the experiments were performed as duplicates or triplicates (n = 3 biologically independent samples, p = 0.000039). Error bars represent standard deviation from the mean. F) The digital photos of a representative mice after various treatments.

3. ELECTRONIC PROPERTIES OF METALLAAROMATICS

3.1 Redox properties

Parallel to studies of electronic absorption and photophysical properties, exploration of redox properties of metallaaromatics has also been progressing towards a more systematic approach. Cyclic voltammograms of ruthenabenzene **41** and bis(ruthenabenzene) **42**, recorded [104] by Xia and co-workers, are shown in Figure 11B. The oxidation wave of **41** can be attributed to the formation of $[Ru(CHC(PPh_3)CHC(PPh_3)CH)Cl_2(PPh_3)_2]^{2+}$. Compared to the electrochemical oxidation behavior of **41**, **42** is very different. **42** is not oxidized in the between −0.50 and +1.00 V (Figure 11B). Two continuous reduction waves of **42** in the negative potential direction indicate that there may be a slight electronic communication between the two metal centers through the chlorido bridges; although, the first wave appears to be irreversible and the complex is clearly electronically asymmetric. This hypothesis still needs to be verified by theoretical calculations and spectroelectrochemical monitoring.

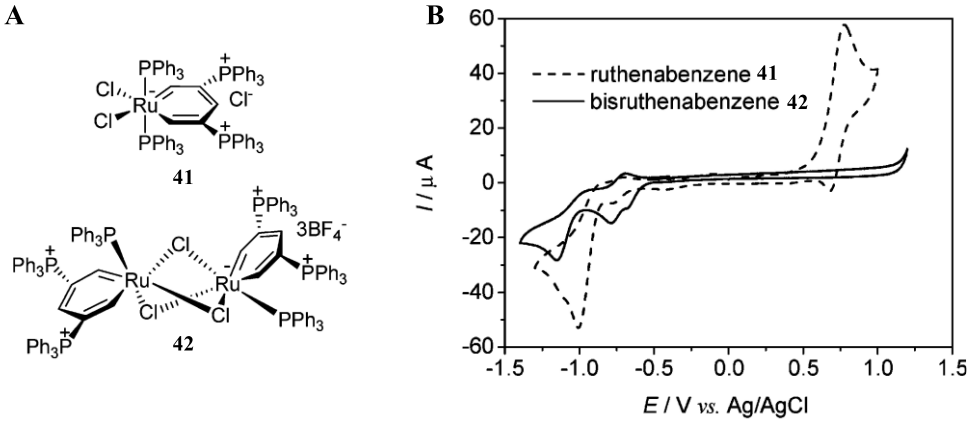

Figure 11. A) Schematic molecular structures of ruthenabenzene **41** and bis(ruthenabenzene) **42**. B) Cyclic voltammograms of **41** and **42** measured in $CH_2Cl_2/10^{-1}$ M Bu_4NClO_4 at a scan rate of 100 mV s^{-1}.

Differently from asymmetric bis(ruthenabenzene) **42**, dinuclear osmabenzenes **43** and **44** (Figure 12), bridged by diisocyanide ligands with an aromatic core R, are symmetric with respect to Os oxidation states.[105] Figure 12A presents their anodic cyclic voltammograms in dichloromethane. The two osmium centers in **43**, with R being the non-conjugated diphenyl ether core, exhibit a relatively weak electronic interaction resulting in the separation of $\Delta E_{1/2}$ = 190 mV between the two reversible

anodic waves. In contrast, complex **44**, with R being the short and conjugated 1,4-phenylene core, exhibits much stronger electronic interaction stabilizing the mixed-valence state, as revealed by the large value of $\Delta E_{1/2}$ = 650 mV. In this case, IR/UV-Vis spectroelectrochemistry combined with DFT/TDDFT calculations would again be a useful tool to study the interesting singly oxidized mixed-valence form in a greater detail. Namely, the existence of several rotamers with a variable degree of electronic interaction between the osmabenzene termini can be envisaged.

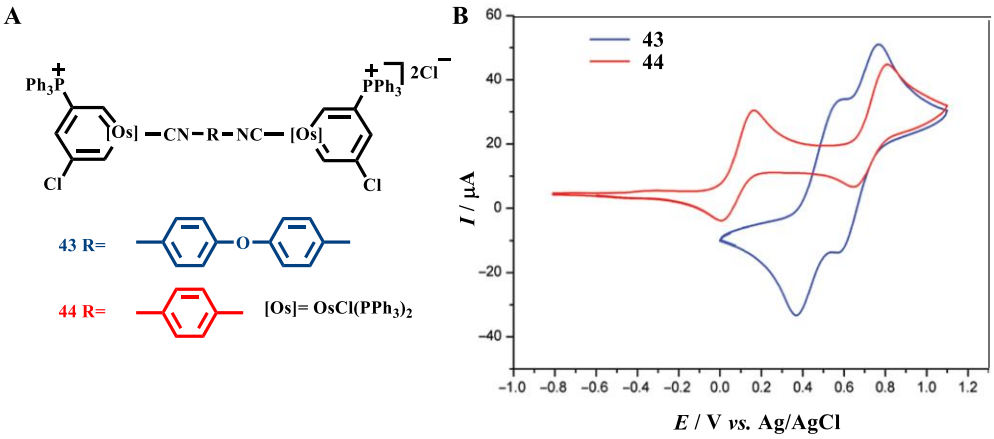

Figure 12. A) Schematic molecular structures of symmetric dinuclear complexes **43** and **44**. B) Positive cyclic voltammograms of **43** and **44** in dichloromethane/10^{-1} M Bu_4NClO_4 recorded at a scan rate of 100 mV s^{-1}.

Also in 2017, heterodinuclear complex **45** with connected osmafuran and ferrocenyl centers was synthesized by a single-step reaction (Figure 13A).[70] Derivatives **46**, **47** and **48** of complex **45** (Figure 13A) were obtained by appropriate ligand substitution reactions. Electrochemical experiments have shown that these compounds exhibit two reversible anodic process in the available potential window, the first oxidation belonging to the Os^{II}/Os^{III} redox couple (Figure 13B, 13C). Corresponding UV-Vis-NIR spectral data and theoretical calculations document that the osmafuran skeleton with the electron-withdrawing phosphonium substituents is not suited as a bridge for intramolecular electron transport in this series. Nonetheless, the results of this study provide a useful theoretical basis for future research on molecular wires encompassing metallacycles and cyclopentadienyl groups as bridging ligands.

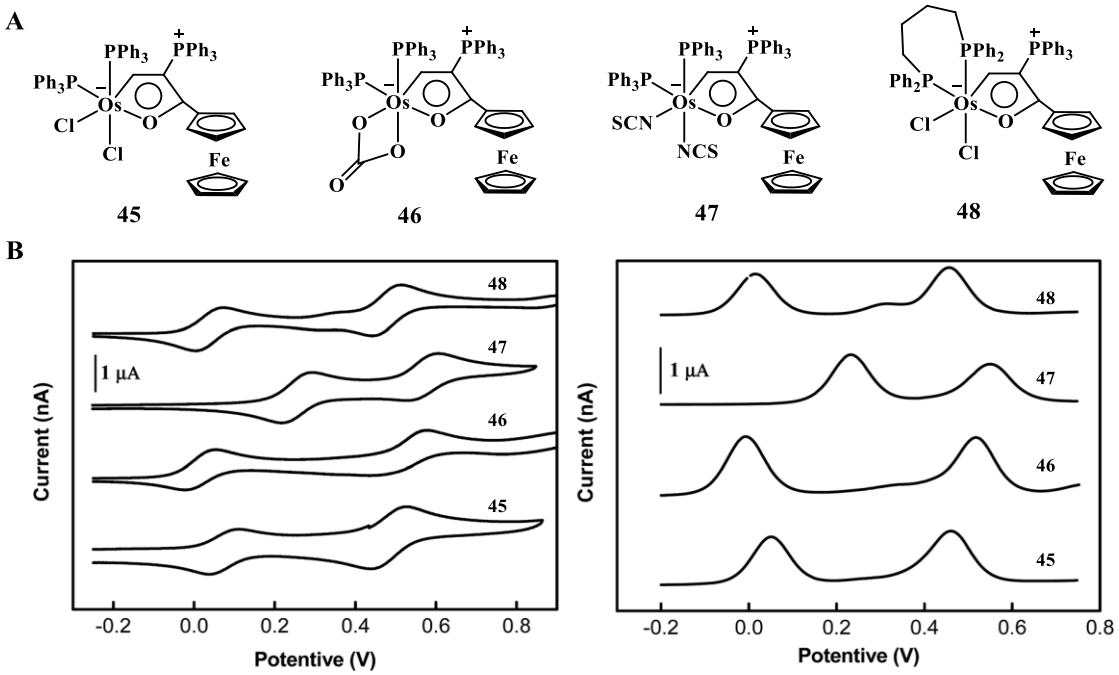

Figure 13. A) Schematic molecular structures of complexes **45**–**48**. B) Cyclic voltammograms of complexes **45**–**48** in CH_2Cl_2/*n*-Bu_4NPF_6 at v = 100 mV s^{-1}. C) Corresponding square-wave voltammograms at f = 10 Hz. Potentials are given relative to the Ag/Ag^+ standard redox couple.

A special part in the section on the phosphonium-stabilized osmanaphthalynes is claimed by complexes **50** and **51** containing a redox-active diphenylamine substituent (Figure 14A).[106] Based on experimental crystallographic data reproduced in DFT-optimized molecular geometries, Liu and coworkers have proven that the diphenylamine-substituted aromatic osmanaphthalynes have an essentially planar, π-delocalized, aromatic cyclic structure, which is advantageous for an intramolecular electron transfer. Therefore, the redox behavior, intramolecular charge-transfer properties and the effect of the diphenylamine unit on the electronic properties of **50** and **51** were thoroughly investigated by UV-Vis absorption spectroscopy, controlled-potential voltammetric methods, UV-vis-NIR spectroelectrochemistry and DFT/TDDFT calculations. The experimental results show that the introduction of the diphenylamine substituent has a large influence on the electronic properties of the target complexes. The low-energy electronic absorption of complexes **50** and **51** is strongly red-shifted compared to that of reference **49**,[107] with the band maxima at 550 nm and ca 3-times higher molar absorptivity (Figure 14B). This characteristic absorption band

corresponds to a dominant HOMO→LUMO charge transfer between the largely diphenylamine-localized HOMO and the Os(-metallacycle)-localized LUMO. The energy gap indeed corresponds well to the value estimated from the voltammetric responses of **50** and **51** (Figure 14C). The spin density in the one-electron-oxidized state is thus mainly distributed at the diphenylamine moiety. The oxidized diphenylamine unit attracts electron density from the metallacycle and $Cl_2Os(PPh_3)$ sites, which is reflected in the NIR electronic absorption of the cationic osmanaphthalynes between 700–1000 nm. The whole osmanaphthalyne metallacycle plays a key role in the process of the electrochemical reduction. In summary, there is an intense CT electronic excitation and non-negligible electronic interaction between the two redox centers linked by osmanaphthalyne ring. Studies of charge transfer between donor and acceptor sites mediated by conjugated metallaring systems, scarcely encountered in the literature so far, are very important for the design and syntheses of new organometallic molecular wires adaptable for future devices, as documented below by the promising osmapentalene-based molecular junctions.

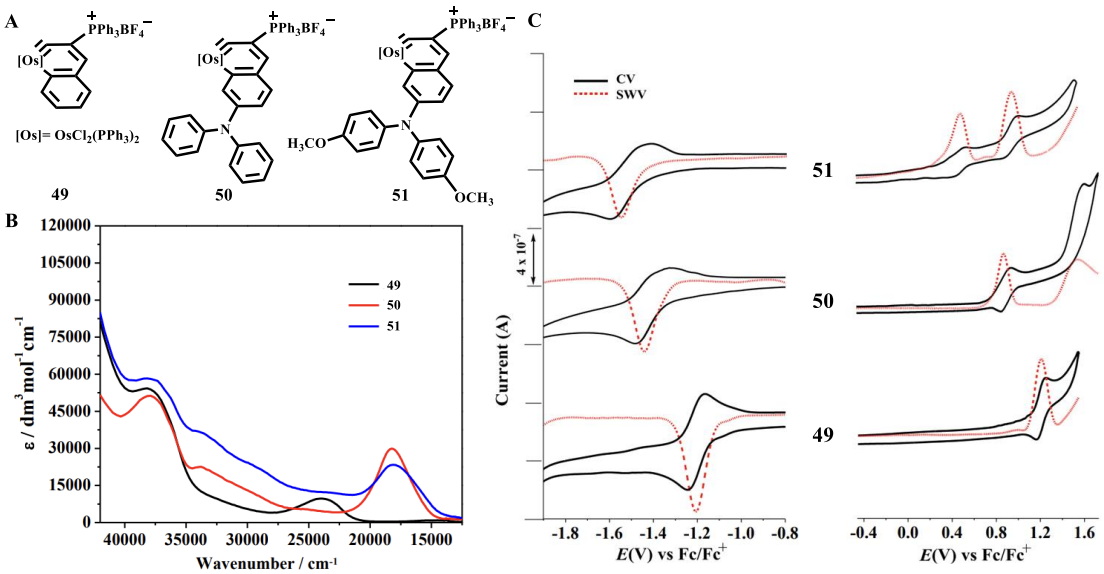

Figure 14. A) Schematic molecular structures of complexes **49**–**51**. B) UV-Vis electronic absorption spectra of **49**–**51** in CH_2Cl_2 at 298 K. C) Left: cyclic voltammograms of complexes **49**–**51** in $CH_2Cl_2/10^{-1}$ M Bu_4NPF_6 at room temperature and $v = 50$ mV s^{-1}. Right: corresponding square-wave voltammograms at $f = 10$ Hz and $t_p = 25$ mV.

In 2022, Liu and co-workers synthesized conjugated dicationic dinuclear

compounds **52** and **53** (Figure 15A) with the aromatic osmapentalene termini connected to the rigid naphthalate bridge by the non-aromatic osmafuran moiety. [108] The downfield proton chemical shifts, AICD analysis, and calculated EDDB values confirmed the aromaticity of the terminal osmapentalene unit and bridge core. Notably, the π-EDDB values (0.687–0.857 *e*) for the osmafuran ring in all these compounds are much smaller than that (2.483 *e*) of furan, revealing the non-aromatic nature of osmafuran rings (Figure 15B). Despite the non-aromatic nature of the osmafuran ring resulting in a small $\Delta E_{1/2}$ potential difference between the two compounds (Figure 15E), electronic communication between the osmapentalene termini can still be observed in the conjugated compound **53**. DFT calculations have demonstrated the effect of the backbones of the two compounds on electronic communication between osmapentalene termini. For **52** the TDDFT data have predicted strong absorption at 498 nm assigned to the HOMO→LUMO excitation within the bis(osmapentalene)-biphenolate backbone π-system, with a limited charge-transfer character. The reason for the weak electronic communication between the osmapentalene termini is the large dihedral angle (35.8°) in the model structure. In contrast, the diosma-octacyclic skeleton of optimized **53** is fully planar (Figure 15C). The broad asymmetric band at 530 nm encompasses two close-lying intense electronic transitions attributed to combined HOMO→LUMO and HOMO−1→LUMO excitations corresponding to transfers of π-electron density from the naphthalenediolate bridge and/or one of the osmapentalene moieties to the other osmapentalene moiety (interpreted as LMCT/MMCT transitions) (Figures 15D and 15F).

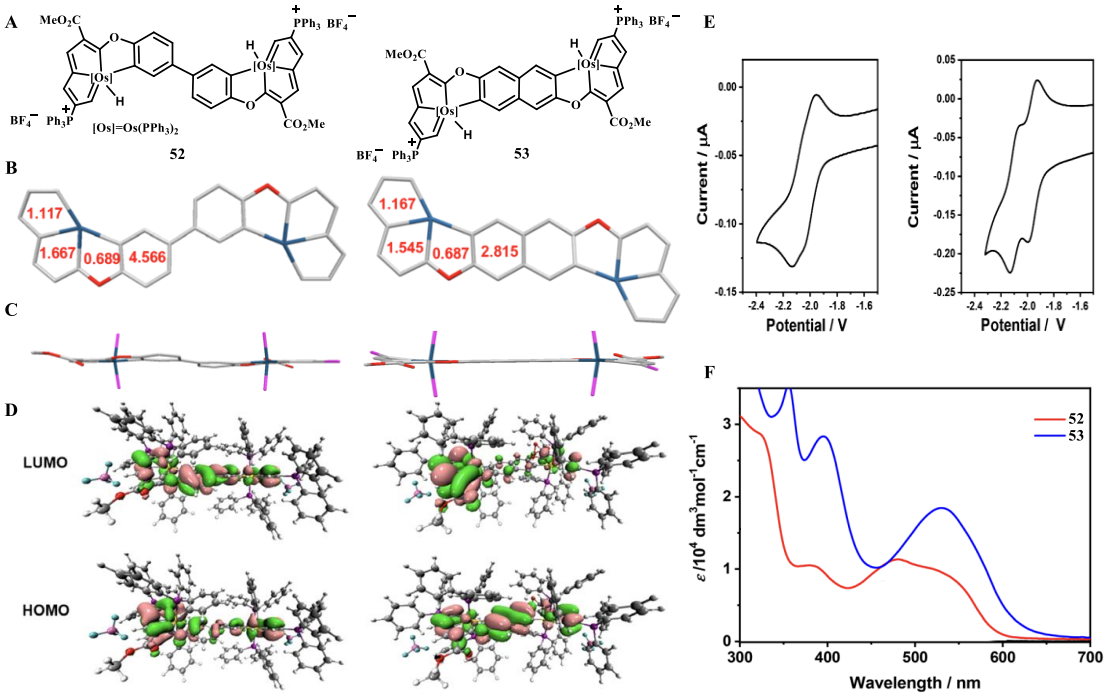

Figure 15. A) Schematic molecular structures of complexes **52** and **53**. B) Separate π-EDDB values for each ring of **52** (left) and **53** (right), including the additional benzene ring in the bridge fused to the osmafuran moiety. C) Crystal structure of **52** (left) and **53** (right) (thermal ellipsoids set at 50% probability); Hydrogen atoms, BF_4^- counter-ions and phenyl substituents in PPh_3 have been omitted for clarity. D) HOMO and LUMO of **52** (left) and **53** (right). E) Cyclic voltammograms of 1 mM **52** (left) and **53** (right) in $CH_2Cl_2/10^{-1}$ M Bu_4NPF_6 at v = 100 mV s^{-1}, T = 233 K. The potential scales correspond to the standard ferrocenium/ferrocene redox couple. F) UV-Vis absorption spectra of **52** and **53** measured in CH_2Cl_2 at T = 293 K.

3.2 Applications

3.2.1 Single-molecule conductors

Interactions between metal centers and organic molecules play a critical role in metal-organic catalysis. Secondary interactions between molecules or atoms arise due to the movement of electrons, being a very weak force that is difficult to measure directly. Thanks to the sensitive current signal of a single molecule in single-molecule electrical techniques, weak secondary interaction and hyperconjugation effects caused by the participation of metal orbitals are made possible by single-molecule electrical techniques. In 2023, molecular wires containing highly strained carbyne **54** designed by the Xia's group realized direct experimental observation of the secondary interaction of metal-organic substances (Figure 16A).[29] By protonation, the highly strained metal−carbon triple bond was converted into metallapentalene **55** containing alternating

conjugated carbene. A shorter Os···C8 distance and a changed orientation of the π plane in the C8–C9 moiety in the single-crystal structure of **55** revealed significant non-planar conformation (Figure 16B). Theoretical calculations have clarified the correlation between this hyperconjugation and non-planar conformation (Figure 16C). The protonation process further strengthens the d_{π}–p_{π} hyperconjugation via an efficient orbital overlap between Os–d_{xy} and p_{π} orbitals. Scanning tunneling microscopy break junction (STM-BJ) characterized the electrical properties of the single-molecule junctions and proved that the electronic properties of single-molecule junctions changed from wire to diode properties before and after protonation, whilst the coupling mode also changed significantly (Figure 16A). This pioneering work has characterized the single-molecule electrical properties of an intra-ring metal carbyne, compared its conductive properties to aromatic hydrocarbons, and demonstrated the great potential of single-molecule electrical techniques for characterizing weak secondary interactions.

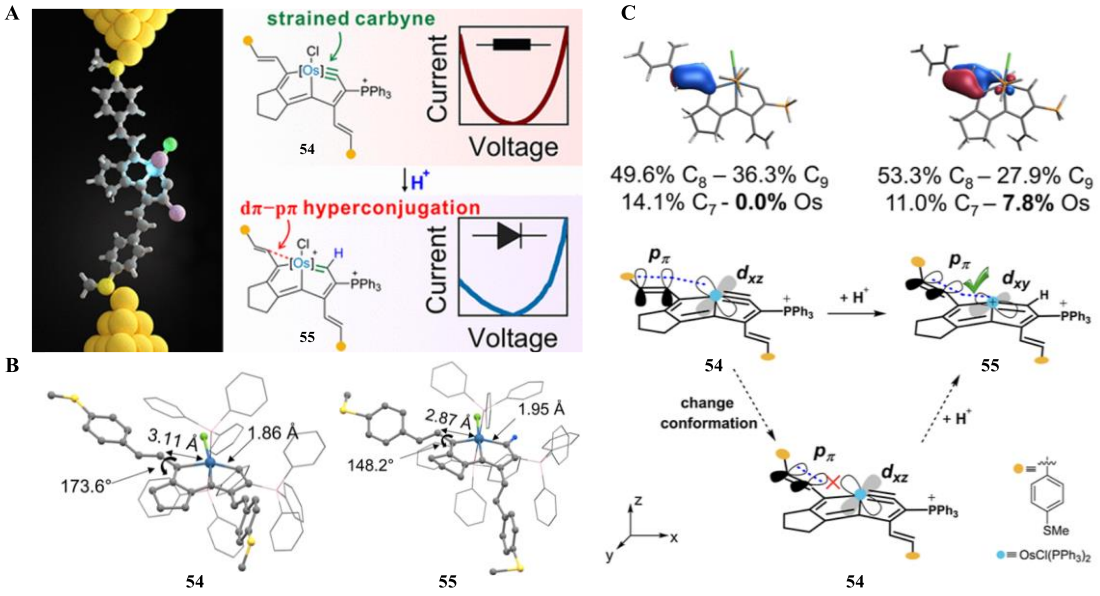

Figure 16. A) Single-molecule electrical characterization of carbolong complexes **54** and **55**. B) Crystal structure of **54** and **55**. C) Theoretical model of metal–carbon hyperconjugation in **54** and **55**.

3.2.2 Solar cells

Strong intermolecular interactions often impede photoluminescence while promoting charge transport. Therefore, the development of organic π conjugated materials with

both semiconductor and luminescent properties remains a difficult problem. In 2023, Xia's group also used PPh_3 ligands in a series of perylene diimide (PDI)-based carbolong complexes **56**–**58** with d_π-p_π conjugation by weakening the function of strong π-π stacking in the PDI core (Figure 17A), resulting in carbolong complexes **56**–**58** exhibiting rare aggregation-induced emission phenomena.[30] These new π-conjugate frameworks are promising electron transport layer (ETL) materials that can be used in high-performance organic solar cells (OSCs). For example, PM6:Y6-based non-fullerene solar cells with complex **58** as an ETL material demonstrated a PCE as high as 17.36% (Figure 17B). This outcome has been attributed to the strong π-π interactions that promote charge transport despite the fact that the PPh_3 ligands are non-planar groups (Figure 17C). The feasibility of exploiting the weakening (strong π-π stacking in the PDI core) and enhancement functions of the PPh_3 ligand (the strong π-π interactions between molecules of the PPh_3 ligand itself) to develop an overall strategy for transforming these novel π-coupled frameworks into multifunctional materials was analyzed favorably. This work highlights new perspectives for the development of organic π-conjugated materials with semiconductor and luminescent properties by introducing non-coplanar π systems.

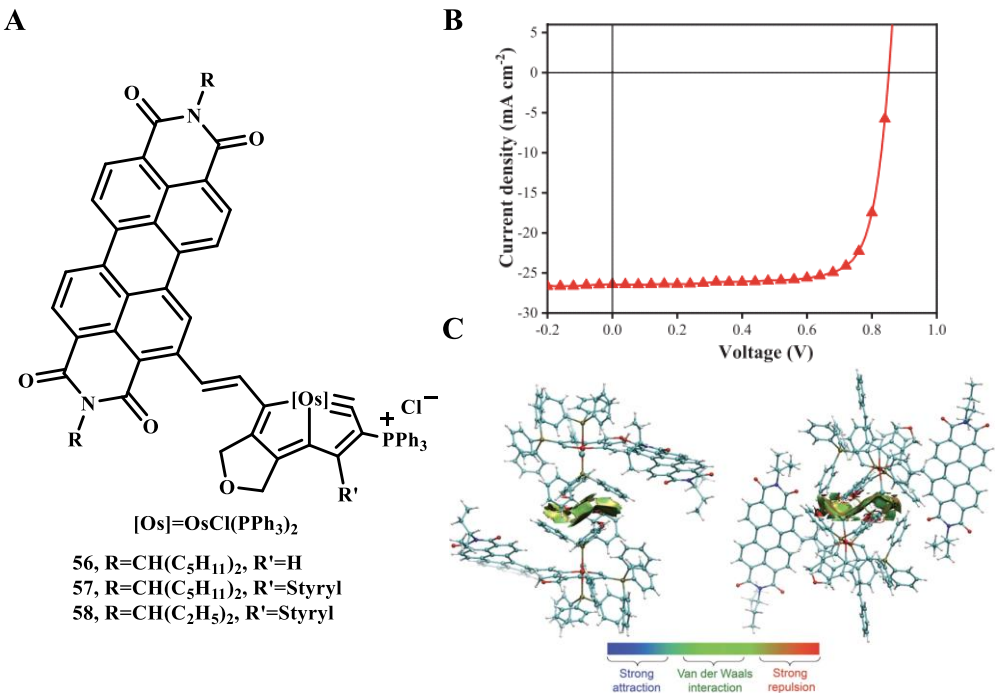

Figure 17. A) Schematic molecular structures of complexes **56**–**58**. B) J–V curve for complex **58** of the characteristics of organic solar cells devices. C) Intermolecular interactions between ligands. NCI plots of π-π interactions of the PPh_3 ligands in the dimer of complex **58**. Grid data were generated with Multiwfn 3.7 and visualized with VMD.[109–110]

4. MAGNETIC PROPERTIES OF METALLAAROMATICS

4.1 Paramagnetic properties

In addition to the spectroscopic, redox and charge-transfer properties reviewed in the preceding sections, some other fundamental physical properties of metallaaromatics are gradually receiving attention, as testified in the recent literature. For example, in 2009, Xia and co-workers reported first osmapyridinium **59** and osmapyridine **60** formed by a formal [4 + 2] cycloaddition reaction (Figure 18)[79], which exhibit unusually low-field ^{1}H NMR signals of OsC*H* and N*H* in **59** and several irregular broad signals in **60**. The above special NMR properties prove that the complexes **59** and **60** are paramagnetic. This is also confirmed by magnetic susceptibility measurements and theoretical calculations. Theoretical calculations show that the triplet states of both **59** and **60** are more stable than the singlet states at the B3LYP level, which deserves further calculating excited-state aromaticity according to Baird's rule.[111]

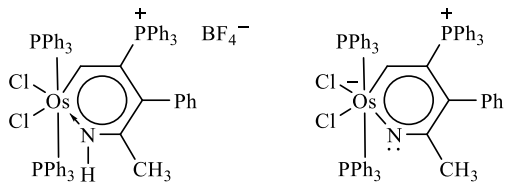

59 **60**

Figure 18. Schematic molecular structures of first osmapyridinium **59** and osmapyridine **60**.

4.2 Excited-state or adaptive aromaticity

According to Hückel's and Baird's rules, aromatic compounds are aromatic in only one state, the first ground state or excited state. Species that are aromatic in both states are named adaptive aromatics, which are extremely rare. In 2019, Zhu's group carried out density functional theory calculations on a series of osmapyridine and osmapyridinium complexes (96 species) and found that in addition to displaying aromaticity only in one state, 2 of them (**61** and **62** in Figure 19) display adaptive aromaticity verified by

various aromaticity indices including HOMA, ELFπ, MCI, ACIDπ plots, and the heat of hydrogenation. Osmapyridinium **62** with phosphonium substituents is the first example with a triplet ground state and adaptive aromaticity in both the lowest triplet and singlet states (Figure 19).[31] Notably, they also demonstrated adaptive aromaticity in 16e and 18e metallapentalenes.[32-33] These efforts may preserve the possibility for the discovery of more organometallics towards photochemical and molecular magnetic applications..

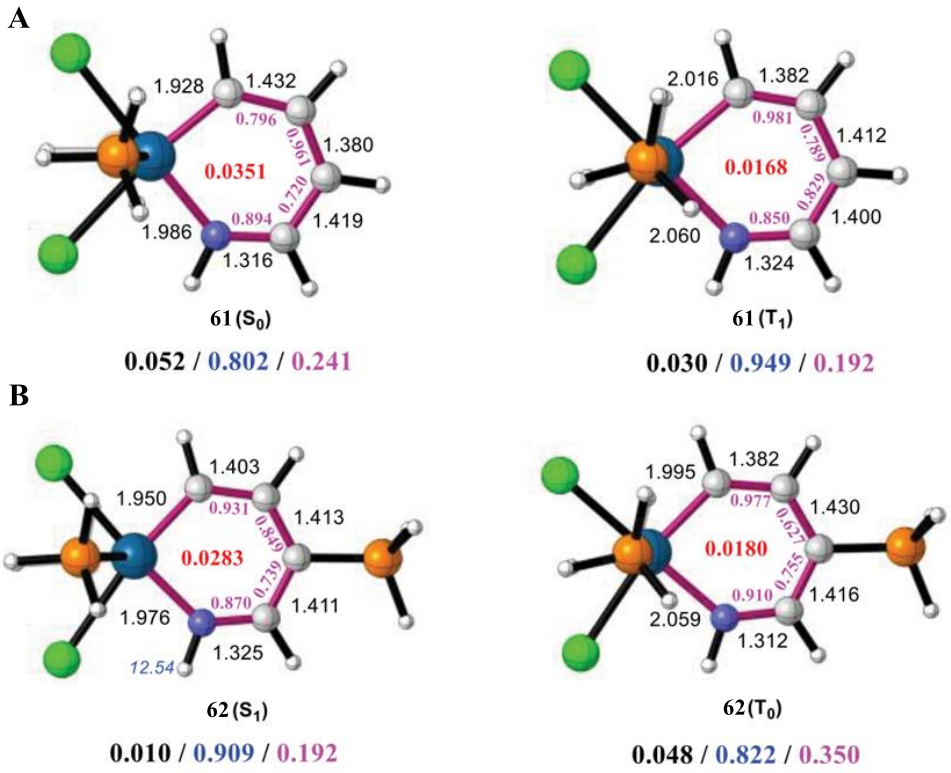

Figure 19. ΔBL (Å, left, black), HOMA (middle, blue), and ΔBV (right, purple) values of osmapyridinium complexes **61** (A) and **62** (B) in the lowest singlet and triplet states. The MCI values (red) are labeled in the center of the ring. The bond lengths (black) and ELF$_\pi$ bifurcation values (purple) are annotated along the bond.

5. CONCLUSIONS AND OUTLOOK

In summary, the recent research into metallaaromatics has proven rewarding to organometallic chemists. Transition metal-containing metallaaromatics not only share the common properties of organic aromatic compounds and transition metal complexes, but also feature their own unique physical properties. Further progress can be achieved

by controlling the metal centers, ring substituents, and co-ligands on the metal. A range of studies reviewed in this work have also shown that metallaaromatics with unconventional photophysics, electronic transport properties and molecular magnetism can be used conveniently in amino acid identification, photothermal effects, functional materials and biomedical fields, but also can be considered as candidates for electron transport layer materials (ETLs) in single-molecule conductors and solar cells.

Looking ahead, the synthesis and application of functional metallaaromatics has been one of the most important and challenging studies in the chemical community. First, it is necessary to pay attention to theoretical calculation to rationally design and develop metallaaromatics. Secondly, the realization of the adaptive aromatity of metallaaromatics is still very difficult, although a variety of metallaaromatics with adaptive aromaticity such as osmapyridinium complexes and metallapentalenes have been predicted, but the specific examples have yet to be synthesized and isolated in the future. Finally, while there are already new synthetic avenues to obtain novel compounds and derivatives with customized properties, viable applications are still the result of the future. Most of the current applied research in this area comes from H. Xia and S. H. Liu and their colleagues, challenging more teams willing to participate in the near future. The examples provided so far clearly show that experimental and theoretical studies of the properties of metallaaromatics and the search for new avenues are worth the efforts.

Acknowledgement

We greatly appreciate the financial support from the National Natural Science Foundation of China (Grant No. 21772054), and the 111 Project B17019 (FH).

ORCID

František Hartl: 0000-0002-7013-5360

References

[1] Kekulé, F. A. Sur la constitution des substances aromatiques. *Bull. Soc. Chim*. **1865**, *3*, 98-111.

[2] Kekulé, F. A. Note sur quelques produits de substitution de la benzine. *Bull. Acad. R. Belg*. **1865**, *19*, 551-563.

[3] (a) Wu, J.; Pisula, W.; Müllen, K. Graphenes as potential material for electronics. *Chem. Rev.* **2007**, *107*, 718-747; (b) Günes, S.; Neugebauer, H.; Sariciftci, N. S. Conjugated polymer-based organic solar cells. *Chem. Rev.* **2007**, *107*, 1324-1338; (c) Shirota, Y.; Kageyama, H. Charge carrier transporting molecular materials and their applications in devices. *Chem. Rev.* **2007**, *107*, 953-1010; (d) Mas-Torrent, M.; Rovira, C. Novel small molecules for organic field-effect transistors: towards processability and high performance. *Chem. Soc. Rev.* **2008**, *37*, 827-838; (e) Grimsdale, A. C.; Chan, K. L.; Martin, R. E.; Jokisz, P. G.; Holmes, A. B. Synthesis of light-emitting conjugated polymers for applications in electroluminescent devices. *Chem. Rev.* **2009**, *109*, 897-1091; (f) Li, C.; Liu, M.; Pschirer, N. G.; Baumgarten, M.; Müllen, K. Polyphenylene-based materials for organic photovoltaics. *Chem. Rev.* **2010**, *110*, 6817-6855; (g) Arias, A. C.; MacKenzie, J. D.; McCulloch, I.; Rivnay, J.; Salleo, A. Materials and applications for large area electronics: solution-based approaches. *Chem. Rev.* **2010**, *110*, 3-24; (h) Figueira-Duarte, T. M.; Müllen, K. Pyrene-based materials for organic electronics. *Chem. Rev.* **2011**, *111*, 7260-7314.

[4] Allard, S.; Forster, M.; Souharce, B.; Thiem, H.; Scherf, U. Organic semiconductors for solution-processable field-effect transistors (OFETs). *Angew. Chem. Int. Ed.* **2008**, *47*, 4070-4098.

[5] Mei, J.; Diao, Y.; Appleton, A. L.; Fang, L.; Bao, Z. Integrated materials design of organic semiconductors for field-effect transistors. *J. Am. Chem. Soc.* **2013**, *135*, 6724-6746.

[6] Thompson, B. C.; Fréchet, J. M. J. Polymer-fullerene composite solar cells. *Angew. Chem. Int. Ed.* **2008**, *47*, 58-77.

[7] Anthony, J. E. The larger acenes: versatile organic semiconductors. *Angew. Chem. Int. Ed.* **2008**, *47*, 452-483.

[8] Kulkarni, A. P.; Tonzola, C. J.; Babel, A.; Jenekhe, S. A. Electron transport materials for organic light-emitting diodes. *Chem. Mater.* **2004**, *16*, 4556-4573.

[9] Yamamoto, T.; Fukushima, T.; Kosaka, A.; Jin, W.; Yamamoto, Y.; Ishii, N.; Aida, T. Conductive one-handed nanocoils by coassembly of hexabenzocoronenes:

control of morphology and helical chirality. *Angew. Chem. Int. Ed.* **2008**, *47*, 1672-1675.

[10] Wang, J.-L.; Zhou, Y.; Li, Y.; Pei, J. Solution-processable gradient red-emitting π-conjugated dendrimers based on benzothiadiazole as core: synthesis, characterization, and device performances. *J. Org. Chem.* **2009**, *74*, 7449-7456.

[11] Wang, J.-L.; Yan, J.; Tang, Z.-M.; Xiao, Q.; Ma, Y.; Pei, J. Gradient shape-persistent π-conjugated dendrimers for light-harvesting: synthesis, photophysical properties, and energy funneling. *J. Am. Chem. Soc.* **2008**, *130*, 9952-9962.

[12] Ma, B.; Woo, C. H.; Miyamoto, Y.; Fréchet, J. M. J. Solution processing of a small molecule, subnaphthalocyanine, for efficient organic photovoltaic cells. *Chem. Mater.* **2009**, *21*, 1413-1417.

[13] Miao, Q. Ten years of *N*-heteropentacenes as semiconductors for organic thin-film transistors. *Adv. Mater.* **2014**, *26*, 5541-5549.

[14] Jiang, W.; Li, Y.; Wang, Z. Heteroarenes as high performance organic semiconductors. *Chem. Soc. Rev.* **2013**, *42*, 6113-6127.

[15] Bosdet, M. J. D.; Jaska, C. A.; Piers, W. E.; Sorensen, T. S.; Parvez, M. Blue fluorescent 4a-aza-4b-boraphenanthrenes. *Org. Lett.* **2007**, *9*, 1395-1398.

[16] Mitsui, C.; Okamoto, T.; Matsui, H.; Yamagishi, M.; Matsushita, T.; Soeda, J.; Miwa, K.; Sato, H.; Yamano, A.; Uemura, T.; Takeya, J. Dinaphtho[1,2-b:2′,1′-d]chalcogenophenes: comprehensive investigation of the effect of the chalcogen atoms in the phenacene-type π-electronic cores. *Chem. Mater.* **2013**, *25*, 3952-3956.

[17] Ball, M.; Zhong, Y.; Wu, Y.; Schenck, C.; Ng, F.; Steigerwald, M.; Xiao, S.; Nuckolls, C. Contorted polycyclic aromatics. *Acc. Chem. Res.* **2015**, *48*, 267-276.

[18] Chen, L.; Mali, K. S.; Puniredd, S. R.; Baumgarten, M.; Parvez, K.; Pisula, W.; Feyter, S. D.; Müllen, K. Assembly and fiber formation of a gemini-type hexathienocoronene amphiphile for electrical conduction. *J. Am. Chem. Soc.* **2013**, *135*, 13531-13537.

[19] Chen, L.; Puniredd, S. R.; Tan, Y.-Z.; Baumgarten, M.; Zschieschang, U.; Enkelmann, V.; Pisula, W.; Feng, X.; Klauk, H.; Müllen K. Hexathienocoronenes: synthesis and self-organization. *J. Am. Chem. Soc.* **2012**, *134*, 17869-17872.

[20] Takase, M.; Enkelmann, V.; Sebastiani, D.; Baumgarten, M.; Müllen, K. Annularly

fused hexapyrrolohexaazacoronenes: an extended π system with multiple interior nitrogen atoms displays stable oxidation states. *Angew. Chem. Int. Ed.* **2007**, *46*, 5524 -5527.

[21] Takase, M.; Narita, T.; Fujita, W.; Asano, M. S.; Nishinaga, T.; Benten, H.; Yoza, K.; Müllen, K. Pyrrole-fused azacoronene family: the influence of replacement with dialkoxybenzenes on the optical and electronic properties in neutral and oxidized states. *J. Am. Chem. Soc.* **2013**, *135*, 8031-8040.

[22] Chen, D. F.; Hua, Y. H.; Xia, H. Metallaaromatic chemistry: history and development. *Chem. Rev.* **2020**, *120*, 12994-13086.

[23] Zhu, C.; Li, S.; Luo, M.; Zhou, X.; Niu, Y.; Lin, M.; Zhu, J.; Cao, Z.; Lu, X.; Wen, T. B.; Xie, Z.; Schleyer, P. v. R.; Xia, H. Stabilization of anti-aromatic and strained five-membered rings with a transition metal. *Nat. Chem*. **2013**, *5*, 698-703.

[24] Lin, R.; Zhang, H.; Li, S.; Chen, L.; Zhang, W.; Wen, T. B.; Zhang, H.; Xia, H. pH-switchable inversion of the metal-centered chirality of metallabenzenes: opposite stereodynamics in reactions of ruthenabenzene with L- and D-cysteine. *Chem. Eur. J*. **2011**, *17*, 2420-2427.

[25] Yang, L.; Zhao, H.; Xie, Y.; Ouyang, P.; Ruan, Y.; Chen, J.; Weng, W.; He, X.; Xia, H. Optically reconfigurable shape memory metallopolymer mediated by a carbolong complex and radically exchangeable covalent bond. *Polym. Chem.* **2022**, *13*, 1844−1851.

[26] Chen, S.; Cao, C.; Yu, Z.; Zhang, A.; Lai, X.; Peng, L.; Hua, Y.; Yang, L.; Jiang, W.; Chen, D.; Wang, Z.; He, F.; Xia H. Conjugated polymers based on metalla-aromatic building blocks. *PNAS*. **2022**, *119*, e2203701119.

[27] Cui, F.-H.; Li, Q.; Gao, L.-H.; Ruan, K.; Ma, K.; Chen, S.; Lu, Z.; Fei, J.; Lin, Y.-M.; Xia, H. Condensed osmaquinolines with NIR-II absorption synthesized by aryl C–H annulation and aromatization. *Angew. Chem. Int. Ed.* **2022**, *61*, e202211734.

[28] Lu, N.; Deng, Z.; Gao, J.; Liang, C.; Xia, H.; Zhang, P. An Osmium-peroxo complex for photoactive therapy of hypoxic tumors. *Nat. Commun*. **2022**, *13*, 2245.

[29] Tang, C.; Jiang, X.-L.; Chen, S.; Hong, W.; Li, J.; Xia, H. Stereoelectronic modulation of a single-molecule junction through a tunable metal-carbon dπ−pπ hyperconjugation. *J. Am. Chem. Soc.* **2023**, *145*, 10404–10410.

[30] Chen, S.; Cao, C.; Yu, Z.; Zhang, A.; Lai, X.; Peng, L.; Hua, Y.; Yang, L.; Jiang, W.; Chen, D.; Wang, Z.; He, F.; Xia, H. A *dπ-pπ* conjugated system with high mobility and strong emission simultaneously. *Adv. Funct. Mater.* **2023**, 2300359.

[31] Shen, T.; Chen, D.; Lin, L.; Zhu, J. Dual aromaticity in both the T0 and S1 states: osmapyridinium with phosphonium substituents. *J. Am. Chem. Soc.* **2019**, *141*, 5720-5727.

[32] Chen, D.; Shen, T.; An, K.; Zhu, J. Adaptive aromaticity in S0 and T1 states of pentalene incorporating 16 valence electron osmium. *Commun. Chem.* **2018**, *1*, 18.

[33] Ye, Q. F.; Fang, Y. F.; Zhu, J. Adaptive aromaticity in 18e metallapentalenes. *Inorg. Chem.* **2023**, *62*, 14764-14772.

[34] Thorn, D. L.; Hoffmann, R. Delocalization in metallocycles. *Nouv. J. Chim.* **1979**, *3*, 39-45.

[35] Elliott, G. P.; Roper, W. R.; Waters, J. M. Metallacyclohexatrienes or 'metallabenzenes.' synthesis of osmabenzene derivatives and X-ray crystal structure of [Os(CSCHCHCHCH)(CO)(PPh_3)$_2$]. *J. Chem. Soc., Chem. Commun*. **1982**, *14*, 811-813.

[36] Huang, Y. Z.; Yang, S. Y.; Li, X. Y. An Investigation of the aromaticity of transition metal heterocyclic complexes by conventional criteria and indices of aromaticity. *J. Organomet. Chem.* **2004**, *689*, 1050-1056.

[37] Cui, M. X.; Lin, R.; Jia, G. C. Chemistry of metallacyclobutadienes. *Chem. - Asian J.* **2018**, *13*, 895-912.

[38] Pedersen, S. F.; Schrock, R. R.; Churchill, M. R.; Wasserman, H. J. Reaction of tungsten(VI) alkylidyne complexes with acetylenes to give tungstenacyclobutadiene and tungsten cyclopentadienyl complexes. *J. Am. Chem. Soc.* **1982**, *104*, 6808-6809.

[39] Bursten, B. E. On the stability of early-transition-netal metallacyclobutadiene complexes. *J. Am. Chem. Soc.* **1983**, *105*, 121-122.

[40] Erdman, F., III; Lawson, D. B. The aromaticity of tungstenacyclobutadiene, $Cl_3W(-ButC-CMe-CMe-)$: a DFT/NICS study. *J. Organomet. Chem.* **2005**, *690*, 4939-4944.

[41] Remya, P. R.; Suresh, C. H. Planar tetracoordinate carbon in tungstenacyclobutadiene from alkyne metathesis and expanded structures. *Dalton Trans.* **2016**, *45*, 1769-1778.

[42] Profilet, R. D.; Fanwick, P. E.; Rothwell, I. P. 1,3-Dimetallabenzene derivatives of niobium or tantalum. *Angew. Chem., Int. Ed. Engl.* **1992**, *31*, 1261-1263.

[43] Riley, P. N.; Profilet, R. D.; Salberg, M. M.; Fanwick, P. E.; Rothwell, I. P. '1,3-Dimetallabenzene' derivatives of niobium and tantalum. *Polyhedron* **1998**, *17*, 773-779.

[44] Zhu, Z.; Wang, X.; Olmstead, M. M.; Power, P. P. Synthesis and characterization of [Ar'GaC(Ph)CH]$_2$ and K_2[Ar'GaC(Ph)CH]$_2$·OEt$_2$: from digallene to digallacyclohexadiene to digallatabenzene. *Angew. Chem. Int. Ed.* **2009**, *48*, 2027-2030.

[45] JRosenthal, U.; Ohff, A.; Michalik, M.; Görls, H.; Burlakov, V. V.; Shur, V. B. Transformation of the first zirconocene alkyne complex without an additional phosphane ligand into a dinuclear σ-alkenyl complex by hydrogen transfer from η^5-C_5H_5 to the alkyne ligand. *Angew. Chem., Int. Ed. Engl.* **1993**, *32*, 1193-1195.

[46] Lv, Z. -J.; Huang, Z.; Shen, J.; Zhang, W. -X.; Xi, Z. Well-defined scandacyclopropenes: synthesis, structure, and reactivity. *J. Am. Chem. Soc.* **2019**, *141*, 20547-20555.

[47] Wei, J.; Zhang, Y.; Chi, Y.; Liu, L.; Zhang, W. -X.; Xi, Z. Aromatic dicupra[10]annulenes. *J. Am. Chem. Soc.* **2016**, *138*, 60-63.

[48] Grande-Aztatzi, R.; Mercero, J. M.; Matito, E.; Frenking, G.; Ugalde, J. M. The aromaticity of dicupra[10]annulenes. *Phys. Chem. Chem. Phys.* **2017**, *19*, 9669-9675.

[49] An, K.; Shen, T.; Zhu, J. Craig-type Möbius aromaticity and antiaromaticity in dimetalla[10]annulenes: a metal-induced yin-and-yang pair. *Organometallics* **2017**, *36*, 3199-3204.

[50] Chen, J.; Jia, G. Recent development in the chemistry of transition metal-containing metallabenzenes and metallabenzynes. *Coord. Chem. Rev.* **2013**, *257*, 2491-2521.

[51] Jia, G. Progress in the chemistry of metallabenzynes. *Acc. Chem. Res.* **2004**, *37*, 479-486.

[52] Jia, G. Recent progress in the chemistry of osmium carbyne and metallabenzyne complexes. *Coord. Chem. Rev.* **2007**, *251*, 2167-2187.

[53] Jia, G. Our journey to the chemistry of metallabenzynes. *Organometallics* **2013**, *32*, 6852-6866.

[54] Bleeke, J. R. Aromatic iridacycles. *Acc. Chem. Res.* **2007**, *40*, 1035-1047.

[55] Frogley, B. J.; Wright, L. J. Recent advances in metallaaromatic chemistry. *Chem. Eur. J.* **2018**, *24*, 2025-2038.

[56] Wang, H.; Zhou, X.; Xia, H. Metallaaromatics containing main-group heteroatoms. *Chin. J. Chem.* **2018**, *36*, 93-105.

[57] Frogley, B. J.; Wright, L. J. Fused-ring metallabenzenes. *Coord. Chem. Rev.* **2014**, *270-271*, 151-166.

[58] Saito, M.; Yoshioka, M. The anions and dianions of group 14 metalloles. *Coord. Chem. Rev.* **2005**, *249*, 765-780.

[59] Ma, W.; Yu, C.; Chen, T.; Xu, L.; Zhang, W.-X.; Xi, Z. Metallacyclopentadienes: synthesis, structure and reactivity. *Chem. Soc. Rev.* **2017**, *46*, 1160-1192.

[60] Wei, J.; Zhang, W.-X.; Xi, Z. The aromatic dianion metalloles, *Chem. Sci.* **2018**, *9*, 560-568.

[61] DeShong, P.; Sidler, D. R.; Rybczynski, P. J.; Slough, G. A.; Rheingold, A. L. A general method for the preparation of carbonyl compounds and butenolides from organomanganese pentacarbonyl complexes. *J. Am. Chem. Soc.* **1988**, *110*, 2575-2585.

[62] Komiya, S.; Ito, T.; Cowie, M.; Yamamoto, A.; Ibers, J. A. Carbon-hydrogen bond activation by transition metal complexes. Oxidative addition of alkyl methacrylate to ruthenium. The structure of hydrido(2-n-butoxycarbonylpropenyl-C1,O) tris(triphenylphosphine)ruthenium (II). *J. Am. Chem. Soc.* **1976**, *98*, 3874-3884.

[63] Padolik, L. L.; Galluci, J. C.; Wojcicki, A. Fischer-type rhenacyclobutadiene complexes: synthesis, structure, and nucleophilic addition/substitution and oxidation reactions. *J. Am. Chem. Soc.* **1993**, *115*, 9986-9996.

[64] Garrett, K. E.; Sheridan, J. B.; Pourreau, D. B.; Feng, W. C.; Geoffroy, G. L.; Staley, D. L.; Rheingold, A. L. Transient generation of the reactive carbene complex $[Cp(CO)_2W{=}CH(Tol)]^+$ and its reactions with alkynes to form vinylcarbene, allyl, naphthol, diene, and metallafuran complexes. *J. Am. Chem. Soc.* **1989**, *111*, 8383-8391.

[65] Grotjahn, D. B.; Hoerter, J. M.; Hubbard, J. L. Double C-H activation during functionalization of phenyl(methyl)ketene on iridium(I) using alkynes. synthesis of 1,4-dien-3-ones. *J. Am. Chem. Soc.* **2004**, *126*, 8866-8867.

[66] Eguillor, B.; Esteruelas, M. A.; Oliván, M.; Oñate, E. C(sp^2)-H activation of RCHE-py (E = CH, N) and RCHCHC(O)R' substrates promoted by a highly

unsaturated osmium-monohydride complex. *Organometallics* **2005**, *24*, 1428-1438.

[67] Buil, M. L.; Esteruelas, M. A.; Garcés, K.; Oliván, M.; Oñate, E. $C_{\beta}(sp^2)$-H bond activation of α, β-unsaturated ketones promoted by a hydride-elongated dihydrogen complex: formation of osmafuran derivatives with carbene, carbyne, and NH-tautomerized α-substituted pyridine ligands. *Organometallics* **2008**, *27*, 4680-4690.

[68] Lin, Y.; Gong, L.; Xu, H.; He, X.; Wen, T. B.; Xia, H. Nine-membered osmacycles derived from metathesis reactions between alkynes and an osmafuran. *Organometallics* **2009**, *28*, 1524-1533.

[69] Liu, B.; Zhao, Q.; Wang, H.; Zeng, B.; Cao, X. Y.; Xia, H. Reactivity study of a hydroxyl coordinated osmium vinyl complex $OsCl_2(PPh_3)_2[CH=C(PPh_3)CHPh(OH)]$. *Sci. China Chem.* **2013**, *56*, 1105-1111.

[70] Liu, B.; Guo, C.-L.; Liu, W.-X.; Guo, M.-E.; Yan, F.; Xue, L.-S.; Wang, H.; Liu, C.-L.; Jin, S. Syntheses, structural characterisation and electronic structures of ferrocenyl-osmafuran heterobinuclear organometallic complexes. *Dalton Trans.* **2017**, *46*, 15803-15811.

[71] Bolano, T.; Castarlenas, R.; Esteruelas, M. A.; Oñate, E. Assembly of an allenylidene ligand, a terminal alkyne, and an acetonitrile molecule: formation of osmacyclopentapyrrole derivatives. *J. Am. Chem. Soc*. **2006**, *128*, 3965-3973.

[72] Esteruelas, M. A.; Masamunt, A. B.; Oliván, M.; Oñate, E.; Valencia, M. Aromatic diosmatricyclic nitrogen-containing compounds. *J. Am. Chem. Soc*. **2008**, *130*, 11612-11613.

[73] Lu, G.-L.; Roper, W. R.; Wright, L. J.; Clark, G. R. A 2-iridathiophene from reaction between $IrCl(CS)(PPh_3)_2$ and $Hg(CH=CHPh)_2$. *J. Organomet. Chem*. **2005**, *690*, 972-981.

[74] Bleeke, J. R.; Ortwerth, M. F.; Chiang, M. Y. Electrophilic addition to an iridathiacyclopentene complex. Synthesis of the first metallathiophene. *Organometalllics* **1993**, *12*, 985-987.

[75] Bleeke, J. R.; Ortwerth, M. F.; Rohde, A. M. Thiapentadienyl-iridium-phosphine chemistry. *Organometallics* **1995**, *14*, 2813-2826.

[76] Bleeke, J. R.; Xie, Y. F.; Peng, W. J.; Chiang, M. Metallabenzene: synthesis, structure, and spectroscopy of a l-irida-3,5-dimethylbenzene complex. *J. Am. Chem. Soc.* **1989**, *111*, 4118-4120.

[77] Bleeke, J. R.; Haile, T.; New, P. R.; Chiang, M. Y. Oxapentadienyl–iridium–phosphine chemistry. synthesis of oxygen-containing iridacycles via C-H bond activation. *Organometallics* **1993**, *12*, 517-528.

[78] Bleeke, J. R.; Haile, T.; New, P. R.; Chiang, M. Y. Oxapentadienyl−iridium−phosphine chemistry. synthesis of oxygen-containing iridacycles via C-H bond activation. *Organometallics* **1993**, *12*, 517−528.

[79] Liu, B.; Wang, H.; Xie, H.; Zeng, B.; Chen, J.; Tao, J.; Wen, T. B.; Cao, Z.; Xia, H. Osmapyridine and osmapyridinium from a formal [4+2] cycloaddition reaction. *Angew. Chem. Int. Ed*. **2009**, *48*, 5430-5434.

[80] Bleeke, J. R.; Hinkle, P. V.; Rath, N. P. Synthesis, structure, spectroscopy, and reactivity of a metallathiabenzene. *J. Am. Chem. Soc*. **1999**, *121*, 595-596.

[81] Bianchini, C.; Meli, A.; Peruzzini, M.; Vizza, F.; Frediani, P.; Herrera, V. Sanchez-Delgado R. A. Opening, desulfurization, and hydrogenation of thiophene at iridium. an experimental study in a homogeneous phase. *J. Am. Chem. Soc*. **1993**, *115*, 2731-2742.

[82] Chen, J.; Daniels, L. M.; Angelici, R. J. New modes of thiophene coordination and reactivity: structures of $Cp^*Ir(\eta^2$-thiophene), an iridathiabenzene, and $Cp^*Ir(\eta^4$-thiophene•BH_3). *J. Am. Chem. Soc*. **1990**, *112*, 199-204.

[83] White, C. J.; Angelici, R. J.; Choi, M.-G. Synthesis, reactions, and ^{77}Se NMR studies of η^5-selenophene complexes of chromium, manganese, ruthenium, and iridium. *Organometallics* **1995**, *14*, 332-340.

[84] Wang, T.; Zhang, H.; Han, F.; Lin, R.; Lin, Z.; Xia, H. Synthesis and characterization of a metallapyridyne complex. *Angew. Chem. Int. Ed.* **2012**, *51*, 9838-9841.

[85] Feng, S. G.; White, P. S.; Templeton, J. L. Amine addition to coordinated nitriles in tungsten(II) alkyne complexes. *Organometallics* **1993**, *12*, 1765-1774.

[86] Perera, T. H.; Lord, R. L.; Heeg, M. J.; Schlegel, H. B.; Winter, C. H. Metallapyrimidines and metallapyrimidiniums from oxidative addition of pyrazolate N–N bonds to niobium(III), niobium(IV), and tantalum(IV) metal centers and assessment of their aromatic character. *Organometallics* **2012**, *31*, 5971-5974.

[87] Psciuk, B. T.; Lord, R. L.; Winter, C. H.; Schlegel, H. B. Can metallapyrimidines be aromatic? a computational study into a new class of metallacycles. *J. Chem. Theory Comput.* **2012**, *8*, 4950-4959.

[88] Mang, A.; Rotthowe, N.; Beltako, K.; Linseis, M.; Pauly, F.; Winter, R. F. Single-molecule conductance studies on quasi- and metallaaromatic dibenzoylmethane coordination compounds and their aromatic analogs. *Nanoscale*. **2023**, *15*, 5305-5316.

[89] Fernández, I.; Frenking, G.; Merino, G. Aromaticity of metallabenzenes and related compounds. *Chem. Soc. Rev.* **2015**, *44*, 6452-6463.

[90] Wright, L. J. *Metallabenzenes: An Expert View*; John Wiley & Sons Ltd: Hoboken, NJ, **2017**.

[91] Zhu, Q.; Chen, S. W; Chen, D. D.; Lin, L.; Xiao, K.; Zhao, L.; Solà, M.; Zhu, J. The application of aromaticity and antiaromaticity to reaction mechanisms. *Fundam. res.* **2023**, 2667-3258.

[92] Luo, M.; Chen, D. F.; Li, Q.; Xia, H. P. Unique properties and emerging applications of carbolong metallaaromatics. *Acc. Chem. Res.* **2023**, *56*, 924-937.

[93] Lin, R.; Zhang, H.; Li, S.; Wang, J.; Xia, H. New highly stable metallabenzenes via nucleophilic aromatic substitution reaction. *Chem. Eur. J*. **2011**, *17*, 4223-4231.

[94] Yuan, W. Z.; Lu, P.; Chen, S.; Lam, J. W.; Wang, Z.; Liu, Y.; Kwok, H. S.; Ma, Y.; Tang, B. Z. Changing the behavior of chromophores from aggregation-caused quenching to aggregation-induced emission: development of highly efficient light emitters in the solid state. *Adv. Mater*. **2010**, *22*, 2159-2163.

[95] Huang, Z.-A.; Lan, Q.; Hua, Y.; Chen, Z.; Zhang, H.; Lin, Z.; Xia, H. Color-tuning strategy for iridapolycycles $[(N^{\wedge}N)Ir(C^{\wedge}C)ClPPh_3]^+$ by the synergistic modifications on both the C^C and N^N units. *Organometallics* **2017**, *36*, 4802-4809.

[96] Zhuo, Q.; Zhang, H.; Hua, Y.; Kang, H.; Zhou, X.; Lin, X.; Chen, Z.; Lin, J.; Zhuo, K.; Xia, H. Constraint of a ruthenium-carbon triple bond to a five-membered ring. *Sci. Adv*. **2018**, *4*, eaat0336.

[97] Huang, H.; Banerjee, S.; Qiu, K.; Zhang, P.; Blacque, O.; Malcomson, T.; Paterson, M. J.; Clarkson, G. J.; Staniforth, M.; Stavros, V. G.; Gasser, G.; Chao, H.; Sadler, P. J. Targeted photoredox catalysis in cancer cells. *Nat. Chem*. **2019**, *11*, 1041–1048.

[98] Lv, W.; Zhang, Z.; K. Y.; Yang, H.; Liu, S.; Xu, A.; Guo, S.; Zhao, Q.; Huang, W. A mitochondria-targeted photosensitizer showing improved photodynamic therapy effects under hypoxia. *Angew. Chem. Int. Ed*. **2016**, *55*, 9947–9951.

[99] Guo, S.; Han, M.; Chen, R.; Zhuang, Y.; Zou, L.; Liu, S.; Huang, W.; Zhao, Q. Mitochondria-localized iridium(III) complexes with anthraquinone groups as effective photosensitizers for photodynamic therapy under hypoxia. *Sci. China Chem*. **2019**, *62*, 1639–1648.

[100] Novohradsky, V.; Rovira, A.; Hally, C.; Galindo, A.; Vigueras, G.; Gandioso, A.; Svitelova, M.; Bresolí-Obach, R.; Kostrhunova, H.; Markova, L.; Kasparkova, J.; Nonell, S.; Ruiz, J.; Brabec, V.; Marchan, V. Towards novel photodynamic anticancer agents generating superoxide anion radicals: a cyclometalated Ir(III) complex conjugated to a far-red emitting coumarin. *Angew. Chem. Int. Ed*. **2019**, *58*, 6311–6315.

[101] Nam, J. S.; Kang, M.-G.; Kang, J.; Park, S.-Y.; Lee, S. J. C.; Kim, H.-T.; Seo, J. K.; Kwon, O.-H.; Lim, M. H.; Rhee, H.-W.; Kwon, T.-H. Endoplasmic reticulum-localized iridium(III) complexes as efficient photodynamic therapy agents via protein modifications. *J. Am. Chem. Soc*. **2016**, *138*, 10968–10977.

[102] Bevernaegie, R.; Doix, B.; Bastien, E.; Diman, A.; Decottignies, A.; Feron, O.; Elias, B. Exploring the phototoxicity of hypoxic active iridium(III)-based sensitizers in 3D tumor spheroids. *J. Am. Chem. Soc*. **2019**, *141*, 18486–18491.

[103] Kuang, S.; Sun, L.; Zhang, X.; Liao, X.; Rees, T. W.; Zeng, L.; Chen, Y.; Zhang, X.; Ji, L.; Chao, Hui. A mitochondrion-localized two-photon photosensitizer generating carbon radicals against hypoxic tumors. *Angew. Chem. Int. Ed*. **2020**, *59*, 20697–20703.

[104] Zhang, H.; Feng, L.; Gong, L.; Wu, L.; He, G.; Wen, T.; Yang, F.; Xia, H. Synthesis and characterization of stable ruthenabenzenes starting from HC≡CCH(OH)C≡CH. *Organometallics* **2007,** *26*, 2705-2713.

[105] Huang, J.; Lin, R.; Wu, L.; Zhao, Q.; Zhu, C.; Wen, T. B.; Xia, H. Synthesis, characterization, and electrochemical properties of bis(osmabenzenes) bridged by diisocyanides. *Organometallics* **2010**, *29*, 2916-2925.

[106] Zhang, M.-X.; Zhang, J.; Jin, X.; Sun, X.; Yin, J.; Hartl, F.; Liu, S. H. Diphenylamine-substituted osmanaphthalyne complexes: structural, bonding, and

redox properties of unusual donor-bridge-acceptor systems. *Chem. Eur. J.* **2018**, *24*, 18998-19009.

[107] Liu, B.; Xie, H.; Wang, H.; Wu, L.; Zhao, Q.; Chen, J.; Wen, T. B.; Cao, Z.; Xia, H. Selective synthesis of osmanaphthalene and osmanaphthalyne by intramolecular C-H activation. *Angew. Chem. Int. Ed*. **2009**, *48*, 5461-5464.

[108] Hu, Y. X.; Deng, Q.; Ou, Y.-P.; Yang, X.; Zhang, J.; Garrett, E. K.; Zhu, J.; Liu, S. H.; Hartl, F. A conjugated diosma-octacyclic complex and its mixed-valence singly reduced state. *Inorg. Chem. Front.* **2022**, *9*, 5893.

[109] Lu, T.; Chen, F. Multiwfn: A multifunctional wavefunction analyzer. *J. Comput. Chem*. **2012**, *33*, 580.

[110] Humphrey, W.; Dalke, A.; Schulten, K. VMD: Visual molecular dynamics. *J. Mol. Graphics* **1996**, *14*, 33.

[111] Baird, N. C. Quantum organic photochemistry. II. resonance and aromaticity in the lowest 3ππ* state of cyclic hydrocarbons. *J. Am. Chem. Soc.* **1972**, *94*, 4941-4948.